The background of the cover is a complex, abstract pattern. It features a grid of thin, dark lines overlaid on a field of vibrant, glowing green and yellow fractal-like structures. These structures resemble branching, crystalline, or organic forms, creating a sense of depth and complexity. The overall effect is a high-tech, scientific aesthetic.

Marc De Graef

Introduction to
Conventional Transmission
Electron Microscopy

CAMBRIDGE

CAMBRIDGE

more information - www.cambridge.org/9780521620062

This page intentionally left blank

INTRODUCTION TO CONVENTIONAL TRANSMISSION ELECTRON MICROSCOPY

Over the past 70 years transmission electron microscopy has developed into a sophisticated sub-nanometer-resolution imaging technique. This book covers the fundamentals of *conventional* transmission electron microscopy (CTEM) as applied to crystalline solids. Emphasis is on the experimental and computational methods used to quantify and analyze CTEM observations. A supplementary website containing interactive modules and free Fortran source code accompanies the text.

The book starts with the basics of crystallography and quantum mechanics providing a sound mathematical footing in both direct and reciprocal space. The next section deals with the microscope itself: lenses, correction coils, the electron gun, apertures, and electron detectors are all described in terms of the underlying theory. The second half of the book focuses on the dynamical theory of electron scattering in solids, including its applications to perfect and defective crystals, electron diffraction, and phase contrast techniques. Nearly all the electron micrographs in the book are taken from four study materials: Cu-15 at% Al, Ti, GaAs, and BiTiO₃, and detailed instructions for the preparation of thin foils are included. Detailed algorithm descriptions are included for a variety of computational problems, ranging from electron diffraction zone axis patterns to dynamical N -beam Bloch wave simulations.

Important features of this textbook include:

- highly illustrated and contains over 100 homework problems;
- supplementary website containing more than 30 000 lines of Fortran 90 source code;
- on-line interactive modules allowing the reader to try out real-time simulations.

The book is based on a lecture course given by the author in the Department of Materials Science and Engineering at Carnegie Mellon University, and is ideal for advanced undergraduate and graduate students as well as researchers new to the field.

MARC DE GRAEF was born in Antwerp (Belgium) on April 7, 1961. He studied physics at the University of Antwerp, and graduated with a Ph.D. in Physics from the Catholic University of Leuven in 1989. He was a post-doctoral researcher at the University of California at Santa Barbara before becoming a faculty member in the Department of Materials Science and Engineering at Carnegie Mellon University (Pittsburgh, PA). He is currently a Full Professor and co-director of the *J. Earle and*

Mary Roberts Materials Characterization Laboratory, which houses five TEMs and two SEMs. Professor De Graef has published more than 100 papers in reviewed journals, such as: *Ultramicroscopy*, *Micron*, *Journal of Microscopy*, *Philosophical Magazine*, *Physical Review*, *Journal of Applied Physics*, *Acta Materialia*, *Scripta Materialia*, and the *Journal of Solid State Chemistry*. In 1996 he received the George Tallman Ladd Research Award from the CMU Engineering College, and in 1998 he received the R.E. Peterson Award from the Society for Experimental Mechanics for Best Paper. He has co-edited a book on the characterization of magnetic materials in the series *Experimental Methods in the Physical Sciences* (Academic Press, 2000).

INTRODUCTION TO CONVENTIONAL TRANSMISSION ELECTRON MICROSCOPY

MARC DE GRAEF



CAMBRIDGE
UNIVERSITY PRESS

CAMBRIDGE UNIVERSITY PRESS

Cambridge, New York, Melbourne, Madrid, Cape Town, Singapore, São Paulo

Cambridge University Press

The Edinburgh Building, Cambridge CB2 2RU, United Kingdom

Published in the United States of America by Cambridge University Press, New York

www.cambridge.org

Information on this title: www.cambridge.org/9780521620062

© Marc De Graef 2003

This book is in copyright. Subject to statutory exception and to the provision of relevant collective licensing agreements, no reproduction of any part may take place without the written permission of Cambridge University Press.

First published in print format 2003

ISBN-13 978-0-511-07442-4 eBook (Adobe Reader)

ISBN-10 0-511-07442-5 eBook (Adobe Reader)

ISBN-13 978-0-521-62006-2 hardback

ISBN-10 0-521-62006-6 hardback

ISBN-13 978-0-521-62995-9 paperback

ISBN-10 0-521-62995-0 paperback

Cambridge University Press has no responsibility for the persistence or accuracy of URLs for external or third-party internet websites referred to in this book, and does not guarantee that any content on such websites is, or will remain, accurate or appropriate.

for Pieter and Erika

Contents

<i>Preface</i>	<i>page</i> xiv
<i>Acknowledgements</i>	xix
<i>Figure reproductions</i>	xxi
1 Basic crystallography	1
1.1 Introduction	1
1.2 Direct space and lattice geometry	2
1.2.1 Basis vectors and unit cells	2
1.2.2 The dot product and the direct metric tensor	5
1.3 Definition of reciprocal space	9
1.3.1 Planes and Miller indices	9
1.3.2 The reciprocal basis vectors	10
1.3.3 Lattice geometry in reciprocal space	14
1.3.4 Relations between direct space and reciprocal space	16
1.3.5 The non-Cartesian vector cross product	18
1.4 The hexagonal system	23
1.4.1 Directions in the hexagonal system	24
1.4.2 The reciprocal hexagonal lattice	26
1.5 The stereographic projection	29
1.5.1 Drawing a point	32
1.5.2 Constructing a great circle through two poles	32
1.5.3 Constructing a small circle around a pole	33
1.5.4 Finding the pole of a great circle	34
1.5.5 Measuring the angle between two poles	34
1.5.6 Measuring the angle between two great circles	34
1.6 Crystal symmetry	34
1.6.1 Symmetry operators	35
1.6.2 Mathematical representation of symmetry operators	39
1.6.3 Point groups	42

1.6.4	Families of planes and directions	44
1.6.5	Space groups	46
1.7	Coordinate transformations	47
1.7.1	Transformation rules	48
1.7.2	Examples of coordinate transformations	50
1.7.3	Rhombohedral and hexagonal settings of the trigonal system	53
1.8	Converting vector components into Cartesian coordinates	55
1.9	Crystallographic calculations on the computer	59
1.9.1	Preliminary remarks	59
1.9.2	Implementing the metric tensor formalism	62
1.9.3	Using space groups on the computer	64
1.9.4	Graphical representation of direct and reciprocal space	68
1.9.5	Stereographic projections on the computer	70
1.10	Recommended additional reading	77
	Exercises	77
2	Basic quantum mechanics, Bragg's Law and other tools	79
2.1	Introduction	79
2.2	Basic quantum mechanics	80
2.2.1	Scalar product between functions	81
2.2.2	Operators and physical observables	82
2.2.3	The Schrödinger equation	84
2.2.4	The de Broglie relation	85
2.2.5	The electron wavelength (non-relativistic)	86
2.2.6	Wave interference phenomena	87
2.3	Elements of the special theory of relativity	89
2.3.1	Introduction	89
2.3.2	The electron wavelength (relativistic)	91
2.3.3	Relativistic correction to the governing equation	94
2.4	The Bragg equation in direct and reciprocal space	96
2.4.1	The Bragg equation in direct space	96
2.4.2	The Bragg equation in reciprocal space	98
2.4.3	The geometry of electron diffraction	100
2.5	Fourier transforms and convolutions	103
2.5.1	Definition	103
2.5.2	The Dirac delta-function	105
2.5.3	The convolution product	106
2.5.4	Numerical computation of Fourier transforms and convolutions	108

2.6	The electrostatic lattice potential	111
2.6.1	Elastic scattering of electrons by an individual atom	111
2.6.2	Elastic scattering by an infinite crystal	116
2.6.3	Finite crystal size effects	119
2.6.4	The excitation error or deviation parameter s_g	121
2.6.5	Phenomenological treatment of absorption	122
2.6.6	Atomic vibrations and the electrostatic lattice potential	126
2.6.7	Numerical computation of the Fourier coefficients of the lattice potential	128
2.7	Recommended additional reading	133
	Exercises	134
3	The transmission electron microscope	136
3.1	Introduction	136
3.2	A brief historical overview	137
3.3	Overview of the instrument	138
3.4	Basic electron optics: round magnetic lenses	142
3.4.1	Cross-section of a round magnetic lens	142
3.4.2	Magnetic field components for a round lens	144
3.4.3	The equation of motion for a charged particle in a magnetic field	146
3.4.4	The paraxial approximation	148
3.4.5	Numerical trajectory computation	150
3.4.6	General properties of round magnetic lenses	156
3.4.7	Lenses and Fourier transforms	161
3.5	Basic electron optics: lens aberrations	166
3.5.1	Introduction	166
3.5.2	Aberration coefficients for a round magnetic lens	166
3.6	Basic electron optics: magnetic multipole lenses	174
3.6.1	Beam deflection	176
3.6.2	Quadrupole elements	178
3.7	Basic electron optics: electron guns	179
3.7.1	Introduction	179
3.7.2	Electron emission	179
3.7.3	Electron guns	187
3.7.4	Beam energy spread and chromatic aberration	190
3.7.5	Beam coherence	193
3.7.6	How many electrons are there in the microscope column?	195
3.8	The illumination stage: prespecimen lenses	195
3.9	The specimen stage	199
3.9.1	Types of objective lenses	199

3.9.2	Side-entry, top-entry and special purpose stages	201
3.9.3	The objective lens and electron diffraction geometry	204
3.9.4	Numerical computation of electron diffraction patterns	208
3.9.5	Higher-order Laue zones	211
3.10	The magnification stage: post-specimen lenses	216
3.11	Electron detectors	221
3.11.1	General detector characteristics	221
3.11.2	Viewing screen	227
3.11.3	Photographic emulsions	228
3.11.4	Digital detectors	230
	Exercises	233
4	Getting started	235
4.1	Introduction	235
4.2	The xtalinfo.f90 program	237
4.3	The study materials	238
4.3.1	Material I: Cu-15 at% Al	238
4.3.2	Material II: Ti	241
4.3.3	Material III: GaAs	243
4.3.4	Material IV: BaTiO ₃	250
4.4	A typical microscope session	252
4.4.1	Startup and alignment	252
4.4.2	Basic observation modes	257
4.5	Microscope calibration	272
4.5.1	Magnification and camera length calibration	273
4.5.2	Image rotation	276
4.6	Basic CTEM observations	277
4.6.1	Bend contours	279
4.6.2	Tilting towards a zone axis pattern	282
4.6.3	Sample orientation determination	284
4.6.4	Convergent beam electron diffraction patterns	288
4.7	Lorentz microscopy: observations on magnetic thin foils	291
4.7.1	Basic Lorentz microscopy (classical approach)	291
4.7.2	Experimental methods	293
4.8	Recommended additional reading	300
	Exercises	301
5	Dynamical electron scattering in perfect crystals	303
5.1	Introduction	303
5.2	The Schrödinger equation for dynamical electron scattering	304
5.3	General derivation of the Darwin–Howie–Whelan equations	306
5.4	Formal solution of the DHW multibeam equations	311
5.5	Slice methods	313

5.6	The direct space multi-beam equations	315
5.6.1	The phase grating equation	316
5.6.2	The propagator equation	317
5.6.3	Solving the full direct-space equation	319
5.7	Bloch wave description	320
5.7.1	General solution method	322
5.7.2	Determination of the Bloch wave excitation coefficients	326
5.7.3	Absorption in the Bloch wave formalism	327
5.8	Important diffraction geometries and diffraction symmetry	328
5.8.1	Diffraction geometries	328
5.8.2	Thin-foil symmetry	330
5.8.3	The reciprocity theorem	331
5.9	Concluding remarks and recommended reading	340
	Exercises	343
6	Two-beam theory in defect-free crystals	345
6.1	Introduction	345
6.2	The column approximation	346
6.3	The two-beam case: DHW formalism	348
6.3.1	The basic two-beam equations	348
6.3.2	The two-beam kinematical theory	348
6.3.3	The two-beam dynamical theory	352
6.4	The two-beam case: Bloch wave formalism	361
6.4.1	Mathematical solution	362
6.4.2	Graphical solution	367
6.5	Numerical two-beam image simulations	371
6.5.1	Numerical computation of extinction distances and absorption lengths	371
6.5.2	The two-beam scattering matrix	377
6.5.3	Numerical (two-beam) Bloch wave calculations	382
6.5.4	Example two-beam image simulations	384
6.5.5	Two-beam convergent beam electron diffraction	388
	Exercises	394
7	Systematic row and zone axis orientations	395
7.1	Introduction	395
7.2	The systematic row case	396
7.2.1	The geometry of a bend contour	396
7.2.2	Theory and simulations for the systematic row orientation	398
7.2.3	Thickness integrated intensities	412
7.3	The zone axis case	419
7.3.1	The geometry of the zone axis orientation	420
7.3.2	Example simulations for the zone axis case	422

7.3.3	Bethe potentials	435
7.3.4	Application of symmetry in multi-beam simulations	437
7.4	Computation of the exit plane wave function	439
7.4.1	The multi-slice and real-space approaches	439
7.4.2	The Bloch wave approach	446
7.4.3	Example exit wave simulations	446
7.5	Electron exit wave for a magnetic thin foil	450
7.5.1	The Aharonov–Bohm phase shift	450
7.5.2	Direct observation of quantum mechanical effects	453
7.5.3	Numerical computation of the magnetic phase shift	454
7.6	Recommended reading	458
	Exercises	458
8	Defects in crystals	460
8.1	Introduction	460
8.2	Crystal defects and displacement fields	460
8.3	Numerical simulation of defect contrast images	465
8.3.1	Geometry of a thin foil containing a defect	466
8.3.2	Example of the use of the various reference frames	470
8.3.3	Dynamical multi-beam computations for a column containing a displacement field	474
8.4	Image contrast for selected defects	478
8.4.1	Coherent precipitates and voids	479
8.4.2	Line defects	481
8.4.3	Planar defects	492
8.4.4	Planar defects and the systematic row	511
8.4.5	Other displacement fields	514
8.5	Concluding remarks and recommended reading	515
	Exercises	516
9	Electron diffraction patterns	518
9.1	Introduction	518
9.2	Spot patterns	518
9.2.1	Indexing of simple spot patterns	518
9.2.2	Zone axis patterns and orientation relations	523
9.2.3	Double diffraction	525
9.2.4	Overlapping crystals and Moiré patterns	530
9.3	Ring patterns	535
9.4	Linear features in electron diffraction patterns	537
9.4.1	Streaks	537
9.4.2	HOLZ lines	540
9.4.3	Kikuchi lines	544

9.5	Convergent beam electron diffraction	550
9.5.1	Point group determination	551
9.5.2	Space group determination	554
9.6	Diffraction effects in modulated crystals	556
9.6.1	Modulation types	556
9.6.2	Commensurate modulations	558
9.6.3	Incommensurate modulations and quasicrystals	569
9.7	Diffuse intensity due to short range ordering	571
9.8	Diffraction effects from polyhedral particles	575
	Exercises	584
10	Phase contrast microscopy	585
10.1	Introduction	585
10.1.1	A simple experimental example	586
10.2	The microscope as an information channel	587
10.2.1	The microscope point spread and transfer functions	589
10.2.2	The influence of beam coherence	606
10.2.3	Plug in the numbers	621
10.2.4	Image formation for an amorphous thin foil	626
10.2.5	Alignment and measurement of various imaging parameters	629
10.3	High-resolution image simulations	638
10.4	Lorentz image simulations	641
10.4.1	Example Lorentz image simulations for periodic magnetization patterns	642
10.4.2	Fresnel fringes for non-magnetic objects	648
10.5	Exit wave reconstruction	649
10.5.1	What are we looking for?	649
10.5.2	Exit wave reconstruction for Lorentz microscopy	652
	Exercises	658
10.6	Final remarks	659
<i>Appendix A1</i>	Explicit crystallographic equations	661
<i>Appendix A2</i>	Physical constants	665
<i>Appendix A3</i>	Space group encoding and other software	666
<i>Appendix A4</i>	Point groups and space groups	667
	<i>List of symbols</i>	677
	<i>Bibliography</i>	685
	<i>Index</i>	705

Preface

About 70 years have passed since Ernst Ruska and Max Knoll constructed the first transmission electron microscope in Germany. During that time, the instrument has steadily developed from a microscope that barely matched the resolution of an optical microscope to a sophisticated and indispensable tool for materials research. Our theoretical understanding of the interaction of high-energy electrons with a solid thin foil and the subsequent propagation of those scattered electrons through a complex electron–optical system has also advanced significantly, to the point that, in principle at least, it is now possible to predict and simulate every possible image and imaging mode. The advent of affordable high-speed computing power has much to do with the transition from a qualitative characterization tool to a highly sensitive and quantitative research instrument.

This book has grown out of the lecture notes for the course “Introduction to Electron Optical Methods”, taught every year or so in the Department of Materials Science and Engineering at Carnegie Mellon University (course 27-763, second year graduate level). While partial notes have existed since the Spring of 1993, work on the book itself started in the Summer of 1996. The subsequent publication of several new textbooks in the area of transmission electron microscopy (TEM)[†] has served to focus the topics treated in this text, and a significant effort was made to provide an approach that would be different from but complementary to the other new texts.

On a regular basis, the journal *Ultramicroscopy* publishes an article by Peter W. Hawkes, who reviews various publications in the field of TEM-based research and closely related fields. I would recommend that the microscopy student take a

[†] Among others: *Transmission Electron Microscopy, a textbook for Materials Science*, by D.B. Williams and C.B. Carter [WC96]; *Advanced Computing in Electron Microscopy*, by E.J. Kirkland [Kir98]; *Transmission Electron Microscopy and Diffractometry of Materials*, by B. Fultz and J.M. Howe [FH01].

look at one of those articles[†] to gain some appreciation of the breadth and depth of the work carried out in the international microscopy community. It is very difficult to cover a similar breadth in an introductory textbook. I have, therefore, limited the topics introduced in this book to a very small subset of all available topics. This book covers only *conventional* TEM techniques; in my interpretation, conventional is equivalent to “non-analytical”, meaning that the book deals only with images and diffraction patterns formed by the primary electrons themselves. Analytical methods, such as energy dispersive x-ray spectroscopy and electron energy loss spectroscopy, are not described in this text. Since I have very little personal experience with scanning TEM (STEM) methods, I have also excluded those from the contents of this book.

I have attempted to write a practical and self-contained textbook; self-contained in the sense that nearly all the required background knowledge (crystallography, basic quantum mechanics, etc.) is included in dedicated chapters at the appropriate level; practical in the sense that the microscopy student should be able to take this book to the microscope (or computer) and follow its guidelines and descriptions. Nature provides us with a large variety of crystal structures and structural defects. In an introductory book, it would not be practical nor desirable to simply show image after image from many different material systems. I have intentionally limited the number of material systems from which electron micrographs are shown. The majority of images are taken from the following four study materials: Cu-15 at% Al, Ti, GaAs, and BaTiO₃. It should not be too difficult for the reader to acquire small amounts of these materials and prepare thin foils. The reader should be able (with some effort) to reproduce nearly every electron micrograph shown in this book. Similarly, extensive Fortran-90 source code is provided on a web site (<http://ctem.web.cmu.edu>); the computer-savvy reader should be able to compile the code and run many different programs related to TEM.

About the structure of this book

Chapters 1 and 2 provide the foundations of crystallography and quantum mechanics, at the level needed later on in the book. Many additional topics are covered in Chapter 2: wave interference, the theory of special relativity, the Bragg equation, the Ewald sphere construction, Fourier transforms, convolutions, the Dirac delta function, elastic scattering of electrons, shape functions, the phenomenological

[†] The series of reviews started in 1981; reviews from the past decade can be found in *Ultramicroscopy*, volumes **90**, p. 215 (2002); **87**, p. 213 (2001); **80**, p. 271 (1999); **76**, p. 139 (1999); **75**, p. 115 (1998); **72**, p. 83 (1998); **69**, p. 51 (1997); **65**, p. 239 (1996); **62**, p. 283 (1996); **60**, p. 325 (1995); **56**, p. 337 (1994); **52**, p. 205 (1993); **50**, p. 106 (1993); **49**, p. 436 (1993); **45**, p. 421 (1992).

description of absorption, and the numerical computation of the electrostatic lattice potential. All crystallographic topics in Chapter 1 are accompanied by extensively documented Fortran-90 source code on the web site.

In Chapter 3, the transmission electron microscope is dissected into its major components: lenses, correction coils, the electron gun, apertures, and electron detectors. All components are extensively described in terms of the underlying theory. The microscope is built up one step at a time, starting from a microscope without lenses. This chapter makes use of photographs of the cross-section of a real microscope column. The relation between reciprocal space and the objective lens back focal plane is introduced, along with higher-order Laue zones, and the simulation of electron diffraction zone axis patterns.

Standard operation procedures for the microscope are introduced in Chapter 4, along with the four study materials. For each material, the reader will find the crystallographic information, as well as a description of thin-foil preparation techniques. The second half of this chapter deals with microscope alignment, bright field and dark field imaging, diffraction patterns, microscope calibration, bend contours, stereographic projections as a tool to describe the orientation of the sample in the column, and the basics of convergent beam electron diffraction methods. The chapter concludes with an introduction to the Fresnel and Foucault modes of Lorentz microscopy.

The dynamical theory of electron scattering in solids is then treated extensively in Chapters 5–7. Chapter 5 introduces the standard methods to describe the scattering problem: the Darwin–Howie–Whelan equations, the scattering matrix formalism, the real-space formalism, and the Bloch wave approach. The symmetry of the diffraction process is also extensively investigated, and the 31 diffraction groups are introduced. In Chapter 6, the dynamical equations are solved for the two-beam case, which is the only case for which a general analytical solution exists. The kinematical model is derived, along with the explicit expressions for the two-beam transmitted and scattered amplitudes for the dynamical case. Numerical simulations are introduced, and the absorptive form factor is described, starting from a discussion of thermal diffuse scattering. Convergent beam electron diffraction (CBED) simulations and approximate thickness determination are introduced.

Chapter 7 deals with the full dynamical multi-beam problem, for both the systematic row case and the zone axis case. Solution methods include the scattering matrix approach, the differential equation approach, and the Bloch wave approach. We introduce the concept of thickness-averaged x-ray emission probability. Extensively documented source code is made available for all multi-beam simulations. The final sections of Chapter 7 deal with exit wave simulations (multi-slice, real-space, and Bloch wave), and with the quantum mechanical aspects of Lorentz microscopy.

In Chapter 8, we describe the general theory of defect image simulations, and then apply it to inclusions, dislocations, and various types of planar defects, including stacking faults, anti-phase boundaries, domain boundaries, inversion boundaries, and grain boundaries. In nearly all cases, the numerical images are compared with selected experimental observations. The emphasis of this chapter is on the simulation methodologies. Chapter 9 deals with a large variety of diffraction effects, including: how to index a zone axis pattern, twin patterns, orientation relations, overlapping crystals, double diffraction, Kikuchi and HOLZ lines, convergent beam patterns and crystal symmetry, modulated crystals, short-range order, and polyhedral inclusions.

Finally, in Chapter 10 we introduce phase contrast observation methods. This chapter focuses on the theory of image formation, and describes the microscope transfer function in detail. Point resolution and the information limit are defined, and the mathematical formalism of image formation and simulation is discussed in detail. Examples of high-resolution image simulations are provided, along with the source code to carry out these simulations. Image simulations for Lorentz microscopy are then explained in the context of the theory of phase contrast. The chapter ends with a brief introduction to exit wave reconstruction, as applied to magnetic materials through the transport-of-intensity formalism.

The electron micrographs in this text were all taken by the author, except where noted otherwise. Micrographs were taken on the following microscopes:

- At Carnegie Mellon University: Philips EM420, JEOL 2000EX, JEOL 4000EX;
- At the University of Antwerp: Philips CM20, Philips CM30, JEOL 4000EX.

About the software accompanying this book

It was not easy to decide which programming language to use for the source code accompanying this book. Modern object-oriented languages provide powerful programming environments but are often limited by the fact that relatively few numerical libraries are available. Fortran-77, the most commonly used scientific programming language, does not have dynamical memory allocation mechanisms and has a rather limited set of variable types. Extensive numerical libraries are available, optimized for many different hardware platforms. In the end, I decided to use Fortran-90 for all of the source code. Fortran-90 provides a good compromise between ease of use (the source code is easier to read than Fortran-77) and flexibility in type declarations and dynamical memory allocations. The code can also be linked to existing Fortran-77 libraries. Conversions to other programming languages should pose no major hurdles. The reader will find more than 30 000 lines of Fortran-90 source code on the web site. The code is grouped into two

segments: a library of general routines, called *CTEMsoft*, and a series of programs that use the library routines. The source code is copyrighted using the GNU General Public License and is freely available. Copyright details are posted on the web site.

The book's web site can be found at the following Uniform Resource Locator or URL:

`http://ctem.web.cmu.edu/`

and is available 24 hours a day with occasional brief interruptions for site maintenance.

Many of the examples in the book are accompanied by interactive routines on the web site. Those routines typically require a few input parameters which can be set by the remote user and are then sent to the web server. The server runs the appropriate code, usually a routine written in the Interactive Data Language (IDL). The resulting output is sent back to the browser in the form of a JPEG or GIF document. About two dozen routines are currently available and more will be added in the future. The complete source code of all IDL routines is also available on-line, as well as the interface routines needed to run the entire web site. Those routines are written in the form of ION-scripts (ION = IDL ON the Web).

Software used in the preparation of this book

Some readers might find it interesting to know which software packages were used in the creation of this book. The following list provides the name of the software package, the vendor (for commercial packages), or author. Weblinks to all companies are provided through the book's web site.

- **Commercial packages:** Adobe Illustrator (Adobe); Adobe Photoshop (Adobe); Digital Micrograph 2.5 and 3.3 (Gatan); Interactive Data Language 5.0 (Research Systems); ION 1.1 (Research Systems); Pro Fortran 6.2 (Absoft); Textures (Blue Sky Research); Fortran-90 (Compaq);
- **Shareware packages:** Alpha editor (P. Keleher);
- **Free packages:** fftw (www.fftw.org); \TeX (www.tug.org); PERL 5.0 (www.perl.com); Apache web server (www.apache.org); gVIM editor (www.vim.org); ghostscript (www.aladdin.com).

The web site for this book runs on a dedicated 666 MHz Compaq TRU-64 UNIX workstation located in the author's office.

Acknowledgements

Many people have (knowingly or unknowingly) contributed to this book. I would like to thank all the graduate students who have taken my electron optical methods course at CMU since the Spring of 1993: Kuang-Ti Chang, Thomas Dupuy, Richard Hsu, Dakshinamurthy Kolluru, Yuichiro Nakamura, Balamuralikrishna Ramalingam, Ursula Sadiq, John Henry Scott, Mandyam Sriram, Levent Trabzon, Damien Gallet, Jin Yong Kim, Eric Ott, Patcharin Poosanaas, Min-Seub Shin, Candida Silva, Shiela Woodard, Chun-Te Wu, Xing Chu, Yu-Nu Hsu, Luana Iorio, Xiaoding Ma, Vijay Narayanan, Tao Pan, Eric Rehder, Edward Sanchez, Zhangmin Wang, Wei Yang, Nicholas Biery, Xuemei Gu, Hirofumi Iwanabe, Paul Lee, Ding-Chung Lu, Bryan Molloseau, Zafer Turgut, Andrew Westmeyer, Jie Zou, Amy Bayer, Juajie Chen, Bassem El-Dasher, Dorothy Farrell, Ali Gungor, Ayetekin Hitit, Amy Hsiao, Taehoon Jang, Sangki Jeong, Il-Seok Kim, Vidhya Ramachandran, Matthew Willard, Wayne Archibald, Kai-Chieh Chang, Yoon Suck Choi, Melik Demirel, Daiwon Choi, Hun Jae Chung, Yi Ding, Zhaohui Fan, Jose Garcia Gonzalez, Francis Johnson, Bala Kavaipatti, Srinivasan Kumar, Hwan Soo Lee, Feroz Mohammad, Robert Noonning, Barbara Osgood, Chad Parish, Ritesh Seal, Rajasekaran Swaminathan, Mihaela Tanase, and Shakul Tandon. Through a near-continuous stream of questions and comments they have improved the readability of the text, and on more than one occasion they have given me reason to rewrite an entire section and/or rework an illustration. Any errors that remain in the text are obviously my own, and the reader should feel free to report them through the book's web site.

There is a vast amount of literature on the subject of transmission electron microscopy. I have attempted to keep the number of citations down to a manageable number; a textbook should, in my opinion, not be an exhaustive source of all papers in the field. Consequently, I may have overlooked important work, or perhaps included topics without full citations of *all* seminal papers in that particular area. I would like to apologize to those readers who have contributed significantly to the

knowledge in this field, but do not find their work cited. The omissions do not reflect on the quality of their work, but are a simple consequence of the page limitations of this book.

The final sections of this book were written during the Winter and Spring months of 2001/2002, while I was on a sabbatical stay at the University of Antwerp (EMAT laboratory). I would like to express my gratitude to Jef Van Landuyt, Gustaaf Van Tendeloo, Dirk Van Dyck, and Dominique Schrijvers for their hospitality and friendship. It was nice to return to the place where I started my undergraduate studies in physics in 1979, and to collaborate with my former teachers. I particularly enjoyed the help of and working with Severin Amelinckx, Ann De Belder, André De Munck, Jan Eysermans, Philippe Geuens, Els Jordaens, Jan Neethling, Pavel Potapov, Ludo Rossou, Freddy Schallenberg, Gertie Stoffelen, and Roger Van Ginderen.

I would like to acknowledge the Research Council of the University of Antwerp, the National Science Foundation (NSF), and Carnegie Mellon University for providing me with financial support during the writing of this book.

I would also like to thank several of my colleagues, currently or formerly at CMU, for their support during the many years it has taken me to complete the text: Greg Rohrer, Tresa Pollock, David Laughlin, and Alan Cramb. In particular, I would like to thank Tom Nuhfer, for his continuous support as supervisor of the electron optics facility at CMU. His knowledge of the practical and technological aspects of electron microscopy has had a tremendous influence on my understanding of the field and, therefore, on the contents of this book. Thanks also to Cathy Rohrer, for pointing out style and grammatical errors.

I would like to thank my editors at CUP, Tim Fishlock and Simon Capelin, for their patience. This book has taken me longer to complete than I had originally anticipated, and there was no pressure at all to hurry up and finish it off.

As any junior faculty member in the U.S. will know, it is not easy to combine a family life with a demanding job as a tenure track professor at a research school, and write a textbook during whatever spare time is left over at the end of the day. I would like to thank my wife, Marie, for her patience and understanding during several years of evening and weekend work; without her support I could not have been successful in my academic career.

Last but not least, I dedicate this book to my two young children, who were born after I started writing: Pieter, now five, and Erika, two. It has been a joy to watch their insatiable appetite for learning new things. It is my sincere hope that the reader of this book will experience a similar eagerness and enthusiasm to learn about transmission electron microscopy.

*Antwerpen, Belgium
May 27th, 2002*

M.D.G.

Figure reproductions

I have made an effort to include mostly new figures in this book. A small number of figures were taken from other authors' published or unpublished work, and the following acknowledgements must be made: Dr. Duncan McKie (Fig. 1.17 taken from [MM86]); Dr M. Kersker, JEOL (Fig. 3.2), permission to publish photographs from the cross-section of a JEOL 120 CX (Figs. 3.2, 3.4, 3.19c, 3.20c and d, 3.23b, 3.32, 3.43b, c, and d); Dr B. Armbruster, Gatan, Inc. (Fig. 3.30); The Royal Society and Professor J.W. Steeds, FRS (Tables. 5.1 and 7.2 and Figs. 5.11 and 5.9, taken from [BESR76]); Academic Press, for permission to reproduce most of Chapter 2 of the book *Magnetic Microscopy and its Applications to Magnetic Materials*, edited by the author and Y. Zhu (Figs. 4.26–4.32, 7.32–7.36, and 10.38–10.39).

1

Basic crystallography

1.1 Introduction

In this chapter, we review the principles and basic tools of crystallography. A thorough understanding of crystallography is a prerequisite for anybody who wishes to learn transmission electron microscopy (TEM) and its applications to solid (mostly inorganic) materials. All diffraction techniques, whether they use x-rays, neutrons, or electrons, make extensive use of the concept of *reciprocal space* and, as we shall see repeatedly later on in this book, TEM is a unique tool for directly probing this space. Hence, it is important that the TEM user become as familiar with reciprocal space as with *direct* or *crystal space*.

This chapter will provide a sound mathematical footing for both direct and reciprocal space, mostly in the form of *non-Cartesian vector calculus*. Many textbooks on crystallography approach this type of vector calculus by explicitly stating the equations for, say, the length of a vector, in each of the seven crystal systems. While this is certainly correct, such tables of equations do not lend themselves to direct implementation in a computer program. In this book, we opt for a method which is independent of the crystal system and which can be implemented readily on a computer. We will introduce powerful tools for the computation of geometrical quantities (distances and angles) in both spaces and for a variety of coordinate transformations in and between those spaces. We will also discuss the *stereographic projection* (SP), an important tool for the analysis of electron diffraction patterns and crystal defects. The TEM user should be familiar with these basic tools.

Although many of these tools are available in commercial or public domain software packages, we will discuss them in sufficient detail so that the reader may also implement them in a new program. It is also useful to *understand* what the various menu-items in software programs really mean. We will minimize to the extent that it is possible the number of “black-box” routines used in this book. The reader may download ASCII files containing all of the routines discussed in this

book from the website. All of the algorithms are written in standard Fortran-90, and can easily be translated into C, Pascal, or any of the object-oriented languages (C++, Java, etc.). The user interface is kept simple, without on-screen graphics. Graphics output, if any, is produced in PostScript or TIFF format and can be viewed on-screen with an appropriate viewer or sent to a printer. The source code can be accessed at the Uniform Resource Locator (URL) <http://ctem.web.cmu.edu/>.

1.2 Direct space and lattice geometry

From a purely mathematical point of view, crystallography can be described as *vector calculus in a rectilinear, but not necessarily orthonormal (or even orthogonal) reference frame*. A discussion of crystallographic tools thus requires that we define basic vector operations in a non-Cartesian reference frame. Such operations are the *vector dot product*, the *vector cross product*, the computation of the length of a vector or the angle between two vectors, and so on.

1.2.1 Basis vectors and unit cells

A *crystal structure* is defined as a regular arrangement of atoms decorating a periodic, three-dimensional *lattice*. The lattice is defined as the set of points which is created by all *integer* linear combinations of three *basis vectors* **a**, **b**, and **c**. In other words, the lattice \mathcal{T} is the set of all vectors **t** of the form:

$$\mathbf{t} = u\mathbf{a} + v\mathbf{b} + w\mathbf{c},$$

with (u, v, w) being an arbitrary triplet of integers. We will often denote the basis vectors by the single symbol \mathbf{a}_i , where the subscript i takes on the values 1, 2, and 3. We will restrict ourselves to *right-handed* reference frames; i.e. the mixed product $(\mathbf{a} \times \mathbf{b}) \cdot \mathbf{c} > 0$. The *lattice vector* **t** can then be rewritten as

$$\mathbf{t} = \sum_{i=1}^3 u_i \mathbf{a}_i, \quad (1.1)$$

with $u_1 = u$, $u_2 = v$, and $u_3 = w$. This expression can be shortened even further by introducing the following notation convention, known as the *Einstein summation convention*: *If a subscript occurs twice in the same term of an equation, then a summation is implied over all values of this subscript and the corresponding summation sign need not be written*. In other words, since the subscript i occurs twice on the right-hand side of equation (1.1), we can drop the summation sign and simply write

$$\mathbf{t} = u_i \mathbf{a}_i. \quad (1.2)$$

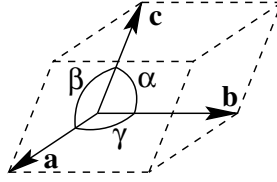


Fig. 1.1. Schematic representation of a general (triclinic or anorthic) unit cell.

The length of a vector is represented by the norm symbol $|\cdot|$; i.e. the length of the basis vector \mathbf{a}_i is $|\mathbf{a}_i|$ with $|\mathbf{a}_1| \equiv a$, $|\mathbf{a}_2| \equiv b$, and $|\mathbf{a}_3| \equiv c$. The angles between the basis vectors are represented by the Greek letters α , β , and γ , as indicated in Fig. 1.1. The six numbers $\{a, b, c, \alpha, \beta, \gamma\}$ are known as the *lattice parameters* of the unit cell.

The lattice parameters can be used to distinguish between the seven *crystal systems*:

$\{a, b, c, \alpha, \beta, \gamma\}$	$a \neq b \neq c; \alpha \neq \beta \neq \gamma$	triclinic or anorthic (a);
$\{a, b, c, \frac{\pi}{2}, \frac{\pi}{2}, \frac{\pi}{2}\}$	$a \neq b \neq c; \beta \neq \frac{\pi}{2}$	monoclinic (m);
$\{a, a, c, \frac{\pi}{2}, \frac{\pi}{2}, \frac{2\pi}{3}\}$	$a = b \neq c$	hexagonal (h);
$\{a, a, a, \alpha, \alpha, \alpha\}$	$a = b = c; \alpha \neq \frac{\pi}{2}$	rhombohedral (R);
$\{a, b, c, \frac{\pi}{2}, \frac{\pi}{2}, \frac{\pi}{2}\}$	$a \neq b \neq c$	orthorhombic (o);
$\{a, a, c, \frac{\pi}{2}, \frac{\pi}{2}, \frac{\pi}{2}\}$	$a = b \neq c$	tetragonal (t);
$\{a, a, a, \frac{\pi}{2}, \frac{\pi}{2}, \frac{\pi}{2}\}$	$a = b = c$	cubic (c).

It is a basic property of a lattice that all lattice sites are equivalent. In other words, any site can be selected as the *origin*. The seven crystal systems give rise to seven *primitive lattices*, since there is only one lattice site per unit cell. We can place additional lattice sites at the endpoints of so-called *centering vectors*; the possible centering vectors are:

$$\mathbf{A} = \left(0, \frac{1}{2}, \frac{1}{2}\right);$$

$$\mathbf{B} = \left(\frac{1}{2}, 0, \frac{1}{2}\right);$$

$$\mathbf{C} = \left(\frac{1}{2}, \frac{1}{2}, 0\right);$$

$$\mathbf{I} = \left(\frac{1}{2}, \frac{1}{2}, \frac{1}{2}\right).$$

A lattice with an extra site at the \mathbf{A} position is known as an *A-centered* lattice, and a site at the \mathbf{I} position gives rise to a *body-centered* or *I-centered* lattice. When the

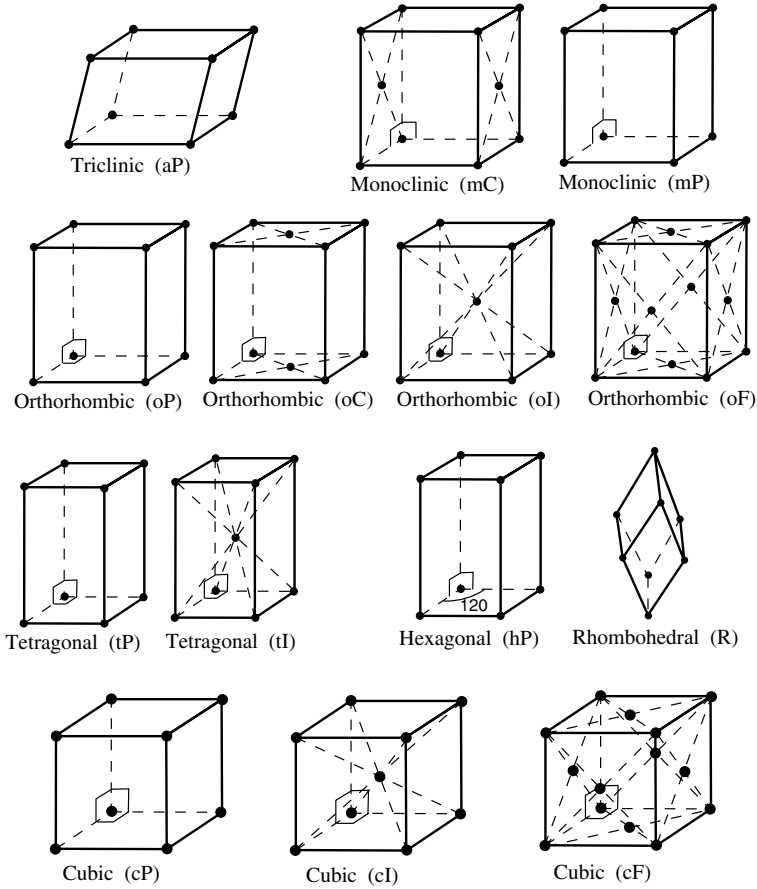


Fig. 1.2. The 14 Bravais lattices and their centering symbols.

three positions, **A**, **B**, and **C**, are simultaneously present as additional lattice sites, the lattice is *face centered* or *F-centered*.

When we combine these centering operations with each of the seven primitive unit cells, seven additional lattices are found. The 14 *Bravais lattices*, first derived by August Bravais in 1850 [Bra50], are shown in Fig. 1.2. They are commonly represented by two-letter symbols, the crystal system symbol followed by a centering symbol: *aP* (primitive anorthic), *mP* (primitive monoclinic), *mC* (C-centered monoclinic), *R* (primitive rhombohedral), *hP* (primitive hexagonal), *oP* (primitive orthorhombic), *oC* (C-centered orthorhombic), *oI* (body-centered orthorhombic), *oF* (face-centered orthorhombic), *tP* (primitive tetragonal), *tI* (body-centered tetragonal), *cP* (primitive cubic), *cI* (body-centered cubic), and *cF* (face-centered cubic). The choice of the lattice parameters of the Bravais lattices follows the conventions listed in the *International Tables for Crystallography, Volume A* [Hah96].

The vector \mathbf{t} in equation (1.1) represents a *direction* in the crystal lattice. It is usually represented by the symbol $[uvw]$ (square brackets, no commas between the components). Negative components are denoted by a minus sign above the corresponding component(s), e.g. $[\bar{u}v\bar{w}]$ for the vector with components $(-u, v, -w)$. Note that there is no agreement in the literature on how to pronounce the symbol $[\bar{u}v\bar{w}]$; some researchers will pronounce the *bar* before the number (i.e. bar u, v, bar w), while others will pronounce it following the number (i.e. u bar, v, w bar). Since one is referring to the negative of a number, and usually this is pronounced as “negative u”, or “minus u”, it makes sense to pronounce the bar *before* the number to which it applies.[†]

The position of an atom inside the unit cell is described by the position vector \mathbf{r} :

$$\mathbf{r} = x\mathbf{a} + y\mathbf{b} + z\mathbf{c} = \sum_{i=1}^3 r_i \mathbf{a}_i = r_i \mathbf{a}_i,$$

where we have again made use of the summation convention. The numbers (x, y, z) are real numbers between 0 and 1, and are known as *fractional coordinates*.

1.2.2 The dot product and the direct metric tensor

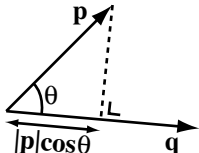
It is important that we have a method of computing distances between atoms and angles between interatomic bonds in the unit cell. Distances in a Cartesian reference frame are typically computed by means of Pythagoras' Theorem: the distance D between two points P and Q with position vectors $\mathbf{p} = (p_1, p_2, p_3)$ and $\mathbf{q} = (q_1, q_2, q_3)$ is given by the length of the vector connecting the two points, or by the square root of the sum of the squares of the differences of the coordinates, i.e.

$$D = \sqrt{(p_1 - q_1)^2 + (p_2 - q_2)^2 + (p_3 - q_3)^2}.$$

In a non-Cartesian reference frame (and almost all crystallographic reference frames are non-Cartesian), this equation is no longer valid and it must be replaced by a more general expression that we shall now derive.

The dot product of two vectors \mathbf{p} and \mathbf{q} can be defined as the product of the lengths of \mathbf{p} and \mathbf{q} multiplied by the cosine of the angle θ between them, or

$\mathbf{p} \cdot \mathbf{q} \equiv |\mathbf{p}||\mathbf{q}| \cos \theta.$



(1.3)

[†] This is merely the author's personal preference. The choice is really up to the reader.

This definition does not depend on a particular choice of reference frame, so it can be taken as a general definition of the dot product. The dot product can be interpreted as the projection of one vector onto a second vector, multiplied by the length of the second vector. If the two vectors are identical, we find (since $\theta = 0$)

$$\mathbf{p} \cdot \mathbf{p} = |\mathbf{p}|^2,$$

from which we derive

$$|\mathbf{p}| = \sqrt{\mathbf{p} \cdot \mathbf{p}}.$$

If the vector \mathbf{p} has components p_i with respect to the crystal basis vectors \mathbf{a}_i , we have[†]

$$|\mathbf{p}| = \sqrt{p_i \mathbf{a}_i \cdot p_j \mathbf{a}_j} = \sqrt{p_i (\mathbf{a}_i \cdot \mathbf{a}_j) p_j} \quad \left(= \sqrt{\sum_{i=1}^3 \sum_{j=1}^3 p_i (\mathbf{a}_i \cdot \mathbf{a}_j) p_j} \right).$$

We see that the *length* of a vector depends on all the dot products between the basis vectors (remember that there are two summations on the right-hand side of this equation!). The quantities $\mathbf{a}_i \cdot \mathbf{a}_j$ are of fundamental importance for crystallographic computations, and they are commonly denoted by the symbol

$$g_{ij} \equiv \mathbf{a}_i \cdot \mathbf{a}_j = |\mathbf{a}_i| |\mathbf{a}_j| \cos \theta_{ij}. \quad (1.4)$$

The nine numbers g_{ij} form a 3×3 matrix which is known as the *direct metric tensor*. From Fig. 1.1, we find that this matrix is given explicitly by

$$g_{ij} = \begin{bmatrix} \mathbf{a} \cdot \mathbf{a} & \mathbf{a} \cdot \mathbf{b} & \mathbf{a} \cdot \mathbf{c} \\ \mathbf{b} \cdot \mathbf{a} & \mathbf{b} \cdot \mathbf{b} & \mathbf{b} \cdot \mathbf{c} \\ \mathbf{c} \cdot \mathbf{a} & \mathbf{c} \cdot \mathbf{b} & \mathbf{c} \cdot \mathbf{c} \end{bmatrix} = \begin{bmatrix} a^2 & ab \cos \gamma & ac \cos \beta \\ ab \cos \gamma & b^2 & bc \cos \alpha \\ ac \cos \beta & bc \cos \alpha & c^2 \end{bmatrix}. \quad (1.5)$$

The matrix g_{ij} is *symmetric*[‡] since $g_{ij} = g_{ji}$. It has only six independent components corresponding to the six lattice parameters $\{a, b, c, \alpha, \beta, \gamma\}$. In other words, the metric tensor contains the same information as the set of lattice parameters, but in a form that allows direct computation of the dot product between two vectors. Explicit expressions for all seven metric tensors are listed in Appendix A1 on page 661.

Example 1.1 A tetragonal crystal has lattice parameters $a = \frac{1}{2} \text{ nm}$ and $c = 1 \text{ nm}$. Compute its metric tensor.

[†] The indices i and j are known as *dummy indices*; it does not really matter which symbols we use for such summation indices, as long as we use them consistently throughout the computation.

[‡] In this textbook, the first subscript of g_{ij} , or any other matrix, will always refer to the rows and the second subscript to the columns of g .

Answer: Substitution of these values into (1.5) results in

$$g_{ij} = \begin{bmatrix} \frac{1}{4} & 0 & 0 \\ 0 & \frac{1}{4} & 0 \\ 0 & 0 & 1 \end{bmatrix}.$$

Note that the units of the metric tensor elements are (nanometer)², but for brevity we usually drop them until the end of a computation.

The length of the vector \mathbf{p} can now be rewritten as

$$|\mathbf{p}| = \sqrt{p_i g_{ij} p_j}.$$

The argument of the square root contains a double summation over i and j . Since i is the row-index of the matrix g_{ij} , and since we can only multiply matrices that are *conformable*,[†] we find that the vector components p_i must be written in row form, while the components p_j must be written in column form, as follows:

$$|\mathbf{p}| = \sqrt{[p_1 \ p_2 \ p_3] \begin{bmatrix} a^2 & ab \cos \gamma & ac \cos \beta \\ ab \cos \gamma & b^2 & bc \cos \alpha \\ ac \cos \beta & bc \cos \alpha & c^2 \end{bmatrix} \begin{bmatrix} p_1 \\ p_2 \\ p_3 \end{bmatrix}}.$$

The dot product between two vectors \mathbf{p} and \mathbf{q} is given by

$$\boxed{\mathbf{p} \cdot \mathbf{q} = p_i \mathbf{a}_i \cdot q_j \mathbf{a}_j = p_i g_{ij} q_j}, \quad (1.6)$$

or explicitly

$$\mathbf{p} \cdot \mathbf{q} = [p_1 \ p_2 \ p_3] \begin{bmatrix} a^2 & ab \cos \gamma & ac \cos \beta \\ ab \cos \gamma & b^2 & bc \cos \alpha \\ ac \cos \beta & bc \cos \alpha & c^2 \end{bmatrix} \begin{bmatrix} q_1 \\ q_2 \\ q_3 \end{bmatrix}.$$

The angle θ between the two vectors is given by (from equation 1.3):

$$\boxed{\theta = \cos^{-1} \left(\frac{\mathbf{p} \cdot \mathbf{q}}{|\mathbf{p}||\mathbf{q}|} \right) = \cos^{-1} \left(\frac{p_i g_{ij} q_j}{\sqrt{p_i g_{ij} p_j} \sqrt{q_i g_{ij} q_j}} \right)}. \quad (1.7)$$

Example 1.2 For the tetragonal crystal in Example 1.1 on page 6, compute the distance between the points $(\frac{1}{2}, 0, \frac{1}{2})$ and $(\frac{1}{2}, \frac{1}{2}, 0)$.

Answer: The distance between two points is equal to the length of the vector connecting them, in this case $(\frac{1}{2} - \frac{1}{2}, 0 - \frac{1}{2}, \frac{1}{2} - 0) = (0, -\frac{1}{2}, \frac{1}{2})$. Using the tetragonal

[†] A matrix \mathcal{A} is said to be conformable with respect to \mathcal{B} if the number of columns in \mathcal{A} equals the number of rows in \mathcal{B} . Matrix multiplication is only defined for conformable matrices.

metric tensor derived previously, we find for the length of this vector:

$$\begin{aligned}
 |\mathbf{p}| &= \sqrt{\begin{bmatrix} 0 & -\frac{1}{2} & \frac{1}{2} \end{bmatrix} \begin{bmatrix} \frac{1}{4} & 0 & 0 \\ 0 & \frac{1}{4} & 0 \\ 0 & 0 & 1 \end{bmatrix} \begin{bmatrix} 0 \\ -\frac{1}{2} \\ \frac{1}{2} \end{bmatrix}}; \\
 &= \sqrt{\begin{bmatrix} 0 & -\frac{1}{2} & \frac{1}{2} \end{bmatrix} \begin{bmatrix} 0 \\ -\frac{1}{8} \\ \frac{1}{2} \end{bmatrix}} = \frac{\sqrt{5}}{4} \text{ nm}.
 \end{aligned}$$

Example 1.3 For the tetragonal unit cell of Example 1.1 on page 6, compute the dot product and the angle between the vectors [120] and [311].

Answer: The dot product is found from the expression for the metric tensor, as follows:

$$\mathbf{t}_{[120]} \cdot \mathbf{t}_{[311]} = [1 \ 2 \ 0] \begin{bmatrix} \frac{1}{4} & 0 & 0 \\ 0 & \frac{1}{4} & 0 \\ 0 & 0 & 1 \end{bmatrix} \begin{bmatrix} 3 \\ 1 \\ 1 \end{bmatrix} = [1 \ 2 \ 0] \begin{bmatrix} \frac{3}{4} \\ \frac{1}{4} \\ 1 \end{bmatrix} = \frac{5}{4} \text{ nm}^2.$$

The angle is found by dividing the dot product by the lengths of the vectors, $|[120]|^2 = \frac{5}{4} \text{ nm}^2$ and $|[311]|^2 = \frac{14}{4} \text{ nm}^2$, from which we find

$$\cos \theta = \frac{\frac{5}{4}}{\sqrt{\frac{14}{4}} \sqrt{\frac{5}{4}}} = \frac{5}{\sqrt{70}} \rightarrow \theta = 53.30^\circ.$$

Example 1.4 The angle between two direct space vectors can be computed in a single operation, instead of using the three individual dot products described in the previous example. Derive a procedure for computing the angle θ based on a 2×3 matrix containing the two vectors \mathbf{p} and \mathbf{q} .

Answer: Consider the following formal relation:

$$\begin{pmatrix} \mathbf{p} \\ \mathbf{q} \end{pmatrix} \cdot (\mathbf{p} \ \mathbf{q}) = \begin{pmatrix} \mathbf{p} \cdot \mathbf{p} & \mathbf{p} \cdot \mathbf{q} \\ \mathbf{q} \cdot \mathbf{p} & \mathbf{q} \cdot \mathbf{q} \end{pmatrix}.$$

The resulting 2×2 matrix contains all three dot products needed for the computation of the angle θ , and only one set of matrix multiplications is needed. We can apply this short cut to the previous example:

$$\begin{pmatrix} 1 & 2 & 0 \\ 3 & 1 & 1 \end{pmatrix} \begin{pmatrix} \frac{1}{4} & 0 & 0 \\ 0 & \frac{1}{4} & 0 \\ 0 & 0 & 1 \end{pmatrix} \begin{pmatrix} 1 & 3 \\ 2 & 1 \\ 0 & 1 \end{pmatrix} = \begin{pmatrix} \frac{5}{4} & \frac{5}{4} \\ \frac{5}{4} & \frac{14}{4} \end{pmatrix},$$

from which we find the same angle of $\theta = 53.30^\circ$.

Note that these equations are valid in every rectilinear coordinate frame[†] and, therefore, in every crystal system. Explicit expressions for distances and angles in the seven reference frames are listed in Appendix A1 on pages 663–664. For a Cartesian, orthonormal reference frame, the metric tensor reduces to the identity matrix. Indeed, the Cartesian basis vectors \mathbf{e}_i have unit length and are orthogonal to each other; therefore, the metric tensor reduces to

$$g_{ij} = \begin{bmatrix} \mathbf{e}_1 \cdot \mathbf{e}_1 & \mathbf{e}_1 \cdot \mathbf{e}_2 & \mathbf{e}_1 \cdot \mathbf{e}_3 \\ \mathbf{e}_2 \cdot \mathbf{e}_1 & \mathbf{e}_2 \cdot \mathbf{e}_2 & \mathbf{e}_2 \cdot \mathbf{e}_3 \\ \mathbf{e}_3 \cdot \mathbf{e}_1 & \mathbf{e}_3 \cdot \mathbf{e}_2 & \mathbf{e}_3 \cdot \mathbf{e}_3 \end{bmatrix} = \begin{bmatrix} 1 & 0 & 0 \\ 0 & 1 & 0 \\ 0 & 0 & 1 \end{bmatrix} \equiv \delta_{ij}, \quad (1.8)$$

where we have introduced the *Kronecker delta* δ_{ij} , which is equal to 1 for $i = j$ and 0 for $i \neq j$. Substitution into equation (1.6) results in

$$\mathbf{p} \cdot \mathbf{q} = p_i \delta_{ij} q_j = p_i q_i = p_1 q_1 + p_2 q_2 + p_3 q_3,$$

which is the standard expression for the dot product between two vectors in a Cartesian reference frame. We will postpone until Section 1.9 a discussion of how to implement the metric tensor formalism on a computer.

1.3 Definition of reciprocal space

In the previous section, we have described how we can compute distances between atoms in a crystal and angles between the bonds connecting those atoms. In Chapter 2, we will see that *diffraction* of electrons is described by the *Bragg equation*, which relates the diffraction angle to the electron wavelength and the spacing between crystal planes. We must, therefore, devise a tool that will enable us to compute this spacing between successive lattice planes in an arbitrary crystal lattice. We would like to have a method similar to that described in the previous section, ideally one with equations identical in form to those for the distance between atoms or the dot product between direction vectors. It turns out that such a tool exists and we will introduce the *reciprocal metric tensor* in the following subsections.

1.3.1 Planes and Miller indices

The description of crystal planes has a long history going all the way back to *René-Juste Haüy* [Häu84] who formulated the *Second Law of Crystal Habit*, also known as the law of simple rational intercepts. This law prompted *Miller* to devise a system to label crystal planes, based on their intercepts with the crystallographic reference axes. Although the so-called *Miller indices* were used by several crystallographers before Miller, they are attributed to him because he used them extensively in his book and teachings [Mil39] and because he developed the familiar *hkl* notation.

[†] They are also valid for curvilinear coordinate frames, but we will not make much use of such reference frames in this book.

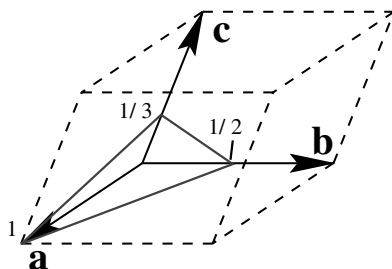


Fig. 1.3. Illustration of the determination of the Miller indices of a plane.

The Miller indices of a plane in an arbitrary crystal system are obtained in the following way.

- (i) If the plane goes through the origin, then displace it so that it no longer contains the origin.
- (ii) Determine the intercepts of the plane with the three basis vectors. Call those intercepts s_1 , s_2 , and s_3 . The intercepts must be measured in units of the basis vector length. For the plane shown in Fig. 1.3, these values are $s_1 = 1$, $s_2 = \frac{1}{2}$, and $s_3 = \frac{1}{3}$. If a plane is parallel to one or more of the basis vectors, then the corresponding intercept value(s) must be taken as ∞ .
- (iii) Invert all three intercepts. For the plane in the figure we find $\frac{1}{s_1} = 1$, $\frac{1}{s_2} = 2$, and $\frac{1}{s_3} = 3$. If one of the intercepts is ∞ , then the corresponding number is zero.
- (iv) Reduce the three numbers to the smallest possible integers (relative primes). (This is not necessary for the example above.)
- (v) Write the three numbers surrounded by round brackets, i.e. (123). This triplet of numbers forms the *Miller indices* of the plane.

In general, the Miller indices of a plane are denoted by the symbol (hkl) . As for directions, negative indices are indicated by a *bar* or minus sign written above the corresponding index, e.g. $(\bar{1}2\bar{3})$. Although Miller indices were defined as relative primes, we will see later on that it is often necessary to consider planes of the type $(nh\ nk\ nl)$, where n is a non-zero integer. All planes of this type are parallel to the plane (hkl) , but for diffraction purposes they are not the same as the plane (hkl) . For instance, the plane (111) is parallel to the plane (222), but the two planes behave differently in a diffraction experiment.

1.3.2 The reciprocal basis vectors

It is tempting to interpret the triplet of Miller indices (hkl) as the components of a vector. A quick inspection of the orientation of the vector $\mathbf{n} = h\mathbf{a} + k\mathbf{b} + l\mathbf{c}$ with respect to the plane (hkl) in an arbitrary crystal system shows that, except

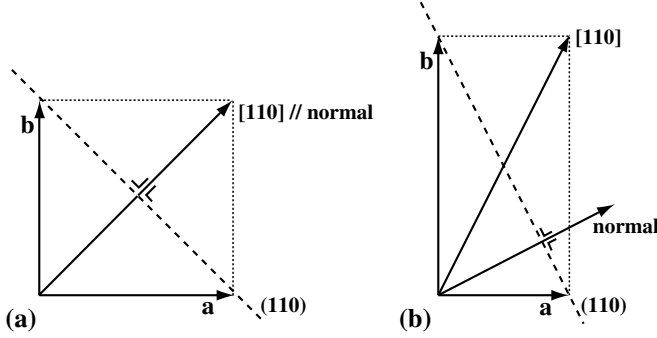


Fig. 1.4. (a) In a cubic (square) lattice, a direction vector $[110]$ is normal to the plane with Miller indices (110) ; this is no longer the case for a non-cubic system, as shown in the rectangular cell (b).

in special cases, there is no fixed relation between the two (see Fig. 1.4). In other words, when the Miller indices are interpreted as the components of a vector with respect to the direct basis vectors \mathbf{a}_i , we do not find a useful relationship between this vector and the plane (hkl) . We must then ask the question: can we find three new basis vectors \mathbf{a}^* , \mathbf{b}^* , and \mathbf{c}^* , related to the direct basis vectors \mathbf{a}_i , such that the vector $\mathbf{g} = h\mathbf{a}^* + k\mathbf{b}^* + l\mathbf{c}^*$ conveys meaningful information about the plane (hkl) ? It turns out that such a triplet of basis vectors exists, and they are known as the *reciprocal basis vectors*. We will distinguish them from the direct basis vectors by means of an asterisk, \mathbf{a}_j^* .

The reciprocal basis vectors can be derived from the following definition:

$$\boxed{\mathbf{a}_i \cdot \mathbf{a}_j^* \equiv \delta_{ij}}, \quad (1.9)$$

where δ_{ij} is the Kronecker delta introduced in equation (1.8). This expression fully defines the reciprocal basis vectors: it states that the vector \mathbf{a}^* must be perpendicular to both \mathbf{b} and \mathbf{c} ($\mathbf{a}^* \cdot \mathbf{b} = \mathbf{a}^* \cdot \mathbf{c} = 0$), and that $\mathbf{a}^* \cdot \mathbf{a} = 1$. The first condition is satisfied if \mathbf{a}^* is parallel to the cross product between \mathbf{b} and \mathbf{c} :

$$\mathbf{a}^* = K(\mathbf{b} \times \mathbf{c}),$$

where K is a constant. The second condition leads to the value of K :

$$\mathbf{a} \cdot \mathbf{a}^* = K \mathbf{a} \cdot (\mathbf{b} \times \mathbf{c}) = 1,$$

from which we find

$$K = \frac{1}{\mathbf{a} \cdot (\mathbf{b} \times \mathbf{c})} \equiv \frac{1}{\Omega},$$

where Ω is the volume of the unit cell formed by the vectors \mathbf{a}_i .

A similar procedure for the remaining two reciprocal basis vectors then leads to the following expressions:

$$\left. \begin{aligned} \mathbf{a}^* &= \frac{\mathbf{b} \times \mathbf{c}}{\mathbf{a} \cdot (\mathbf{b} \times \mathbf{c})}; \\ \mathbf{b}^* &= \frac{\mathbf{c} \times \mathbf{a}}{\mathbf{a} \cdot (\mathbf{b} \times \mathbf{c})}; \\ \mathbf{c}^* &= \frac{\mathbf{a} \times \mathbf{b}}{\mathbf{a} \cdot (\mathbf{b} \times \mathbf{c})}. \end{aligned} \right\} \quad (1.10)$$

We define the *reciprocal lattice* \mathcal{T}^* as the set of end-points of the vectors of the type

$$\mathbf{g} = h\mathbf{a}^* + k\mathbf{b}^* + l\mathbf{c}^* = \sum_{i=1}^3 g_i \mathbf{a}_i^* = g_i \mathbf{a}_i^*,$$

where (h, k, l) are integer triplets. This new lattice is also known as the *dual lattice*, but in the diffraction world we prefer the name *reciprocal lattice*. We will now investigate the relation between the reciprocal lattice vectors \mathbf{g} and the planes with Miller indices (hkl) .

We will look for all the direct space vectors \mathbf{r} with components $r_i = (x, y, z)$ that are perpendicular to the vector \mathbf{g} . We already know that two vectors are perpendicular to each other if their dot product vanishes. In this case we find:

$$0 = \mathbf{r} \cdot \mathbf{g} = (r_i \mathbf{a}_i) \cdot (g_j \mathbf{a}_j^*) = r_i (\mathbf{a}_i \cdot \mathbf{a}_j^*) g_j.$$

We also know from equation (1.9) that the last dot product is equal to δ_{ij} , so

$$\mathbf{r} \cdot \mathbf{g} = r_i \delta_{ij} g_j = r_i g_i = r_1 g_1 + r_2 g_2 + r_3 g_3 = hx + ky + lz = 0. \quad (1.11)$$

The components of the vector \mathbf{r} must satisfy the relation $hx + ky + lz = 0$ if \mathbf{r} is to be perpendicular to \mathbf{g} . This relation represents the equation of a plane through the origin of the direct crystal lattice. If a plane intersects the basis vectors \mathbf{a}_i at intercepts s_i , then the equation of that plane is given by [Spi68]

$$\frac{x}{s_1} + \frac{y}{s_2} + \frac{z}{s_3} = 1, \quad (1.12)$$

where (x, y, z) is an arbitrary point in the plane. The right-hand side of this equation takes on different values when we translate the plane along its normal, and, in particular, is equal to zero when the plane goes through the origin. Comparing

$$hx + ky + lz = 0$$

with

$$\frac{x}{s_1} + \frac{y}{s_2} + \frac{z}{s_3} = 0,$$

we find that the integers h , k , and l are reciprocals of the intercepts of a plane with the direct lattice basis vectors. This is exactly the definition of the *Miller indices* of a plane! We thus find the fundamental result:

The reciprocal lattice vector \mathbf{g} , with components (h, k, l) , is perpendicular to the plane with Miller indices (hkl) .

For this reason, a reciprocal lattice vector is often denoted with the Miller indices as subscripts, e.g. \mathbf{g}_{hkl} .

Since the vector $\mathbf{g} = g_i \mathbf{a}_i^*$ is perpendicular to the plane with Miller indices $g_i = (hkl)$, the unit normal to this plane is given by

$$\mathbf{n} = \frac{\mathbf{g}_{hkl}}{|\mathbf{g}_{hkl}|}.$$

The perpendicular distance from the origin to the plane intersecting the direct basis vectors at the points $\frac{1}{h}$, $\frac{1}{k}$, and $\frac{1}{l}$ is given by the projection of any vector \mathbf{t} ending in the plane onto the plane normal \mathbf{n} (see Fig. 1.5). This distance is also, by definition, the *interplanar spacing* d_{hkl} . Thus,

$$\mathbf{t} \cdot \mathbf{n} = \mathbf{t} \cdot \frac{\mathbf{g}_{hkl}}{|\mathbf{g}_{hkl}|} \equiv d_{hkl}.$$

We can arbitrarily select $\mathbf{t} = \frac{\mathbf{a}}{h}$, which leads to

$$\mathbf{t} \cdot \mathbf{g}_{hkl} = \frac{\mathbf{a}}{h} \cdot (h\mathbf{a}^* + k\mathbf{b}^* + l\mathbf{c}^*) = \frac{\mathbf{a}}{h} \cdot h\mathbf{a}^* = 1 = d_{hkl} |\mathbf{g}_{hkl}|,$$

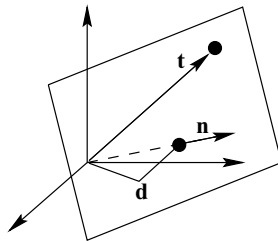


Fig. 1.5. The distance of a plane to the origin equals the projection of any vector \mathbf{t} ending in this plane onto the unit plane normal \mathbf{n} .

from which we find

$$|\mathbf{g}_{hkl}| = \frac{1}{d_{hkl}}. \quad (1.13)$$

The length of a reciprocal lattice vector is equal to the inverse of the spacing between the corresponding lattice planes.

We thus find that every vector \mathbf{g}_{hkl} of the reciprocal lattice is parallel to the normal to the set of planes with Miller indices (hkl) , and the length of \mathbf{g}_{hkl} (i.e. the distance from the point (h, k, l) to the origin of the reciprocal lattice) is equal to the inverse of the spacing between consecutive lattice planes. At this point, it is useful to introduce methods for lattice calculations in the reciprocal lattice; we will see that the metric tensor formalism introduced in Section 1.2.2 can also be applied to the reciprocal lattice.

1.3.3 Lattice geometry in reciprocal space

We know that the length of a vector is given by the square root of the dot product of this vector with itself. Thus, the length of \mathbf{g} is given by

$$\frac{1}{d_{hkl}} = |\mathbf{g}| = \sqrt{\mathbf{g} \cdot \mathbf{g}} = \sqrt{(g_i \mathbf{a}_i^*) \cdot (g_j \mathbf{a}_j^*)} = \sqrt{g_i (\mathbf{a}_i^* \cdot \mathbf{a}_j^*) g_j}.$$

Again we find that the general dot product involves knowledge of the dot products of the basis vectors, in this case the reciprocal basis vectors. We introduce the *reciprocal metric tensor*:

$$g_{ij}^* \equiv \mathbf{a}_i^* \cdot \mathbf{a}_j^*. \quad (1.14)$$

Explicitly, the reciprocal metric tensor is given by:

$$\begin{aligned} g^* &= \begin{bmatrix} \mathbf{a}^* \cdot \mathbf{a}^* & \mathbf{a}^* \cdot \mathbf{b}^* & \mathbf{a}^* \cdot \mathbf{c}^* \\ \mathbf{b}^* \cdot \mathbf{a}^* & \mathbf{b}^* \cdot \mathbf{b}^* & \mathbf{b}^* \cdot \mathbf{c}^* \\ \mathbf{c}^* \cdot \mathbf{a}^* & \mathbf{c}^* \cdot \mathbf{b}^* & \mathbf{c}^* \cdot \mathbf{c}^* \end{bmatrix}; \\ &= \begin{bmatrix} a^{*2} & a^* b^* \cos \gamma^* & a^* c^* \cos \beta^* \\ b^* a^* \cos \gamma^* & b^{*2} & b^* c^* \cos \alpha^* \\ c^* a^* \cos \beta^* & c^* b^* \cos \alpha^* & c^{*2} \end{bmatrix}, \end{aligned} \quad (1.15)$$

where $\{a^*, b^*, c^*, \alpha^*, \beta^*, \gamma^*\}$ are the reciprocal lattice parameters. Explicit expressions for all seven reciprocal metric tensors are given in Appendix A1 on page 662.

In Section 1.3.4, we will develop an easy way to compute the reciprocal basis vectors and lattice parameters; for now the explicit equations in the appendix are sufficient.

Example 1.5 Compute the reciprocal metric tensor for a tetragonal crystal with lattice parameters $a = \frac{1}{2}$ and $c = 1$.

Answer: Substitution of the lattice parameters into the expression for the tetragonal reciprocal metric tensor in Appendix A1 yields

$$\mathbf{g}_{\text{tetragonal}}^* = \begin{bmatrix} 4 & 0 & 0 \\ 0 & 4 & 0 \\ 0 & 0 & 1 \end{bmatrix}.$$

We can now rewrite the length of the reciprocal lattice vector \mathbf{g} as

$$\frac{1}{d_{hkl}} = |\mathbf{g}| = \sqrt{\mathbf{g} \cdot \mathbf{g}} = \sqrt{g_i g_{ij}^* g_j}. \quad (1.16)$$

The angle θ between two reciprocal lattice vectors \mathbf{f} and \mathbf{g} is given by the standard relation (equation 1.7):

$$\theta = \cos^{-1} \left(\frac{f_i g_{ij}^* g_j}{\sqrt{f_i g_{ij}^* f_j} \sqrt{g_i g_{ij}^* g_j}} \right). \quad (1.17)$$

Example 1.6 Compute the angle between the (120) and (311) plane normals for the tetragonal crystal of Example 1.5.

Answer: Substitution of the vector components and the reciprocal metric tensor into the expression for the angle results in

$$\begin{aligned} \cos \theta &= \frac{[1\ 2\ 0] \begin{bmatrix} 4 & 0 & 0 \\ 0 & 4 & 0 \\ 0 & 0 & 1 \end{bmatrix} \begin{bmatrix} 3 \\ 1 \\ 1 \end{bmatrix}}{\sqrt{[1\ 2\ 0] \begin{bmatrix} 4 & 0 & 0 \\ 0 & 4 & 0 \\ 0 & 0 & 1 \end{bmatrix} \begin{bmatrix} 1 \\ 2 \\ 0 \end{bmatrix}} \sqrt{[3\ 1\ 1] \begin{bmatrix} 4 & 0 & 0 \\ 0 & 4 & 0 \\ 0 & 0 & 1 \end{bmatrix} \begin{bmatrix} 3 \\ 1 \\ 1 \end{bmatrix}}}, \\ &= \frac{20}{\sqrt{20 \times 41}} = 0.69843, \\ &\rightarrow \theta = 45.7^\circ. \end{aligned}$$

Example 1.7 Redo the computation of the previous example using the shorthand notation introduced in Example 1.4.

Answer: The matrix product is given by

$$\begin{pmatrix} 1 & 2 & 0 \\ 3 & 1 & 1 \end{pmatrix} \begin{pmatrix} 4 & 0 & 0 \\ 0 & 4 & 0 \\ 0 & 0 & 1 \end{pmatrix} \begin{pmatrix} 1 & 3 \\ 2 & 1 \\ 0 & 1 \end{pmatrix} = \begin{pmatrix} 20 & 20 \\ 20 & 41 \end{pmatrix},$$

from which we find the same angle of $\theta = 45.7^\circ$.

Note that we have indeed managed to create a computational tool that is formally identical to that used for distances and angles in direct space. This should come as no surprise, since the reciprocal basis vectors are just another set of basis vectors, and the equations for direct space must be valid for *any* non-Cartesian reference frame. The particular choice for the reciprocal basis vectors (see equation 1.9) guarantees that they are useful for the description of lattice planes. In the next section, we will derive relations between the direct and reciprocal lattices.

1.3.4 Relations between direct space and reciprocal space

We know that a vector is a mathematical object that exists independently of the reference frame. This means that every vector defined in the direct lattice must also have components with respect to the reciprocal basis vectors and vice versa. In this section, we will devise a tool that will permit us to transform vector quantities back and forth between direct and reciprocal space.

Consider the vector \mathbf{p} :

$$\mathbf{p} = p_i \mathbf{a}_i = p_j^* \mathbf{a}_j^*,$$

where p_j^* are the reciprocal space components of \mathbf{p} . Multiplying both sides by the direct basis vector \mathbf{a}_m , we have

$$\left. \begin{aligned} p_i \mathbf{a}_i \cdot \mathbf{a}_m &= p_j^* \mathbf{a}_j^* \cdot \mathbf{a}_m, \\ p_i g_{im} &= p_j^* \delta_{jm} = p_m^*, \end{aligned} \right\} \quad (1.18)$$

or

$$p_m^* = p_i g_{im}. \quad (1.19)$$

It is easily shown that the inverse relation is given by

$$p_i = p_m^* g_{mi}^*. \quad (1.20)$$

We thus find that *post-multiplication by the metric tensor* transforms vector components from direct space to reciprocal space, and post-multiplication by the reciprocal

metric tensor transforms vector components from reciprocal to direct space. These relations are useful because they permit us to determine the components of a direction vector $\mathbf{t}_{[uvw]}$ with respect to the reciprocal basis vectors, or the components of a plane normal \mathbf{g}_{hkl} with respect to the direct basis vectors.

Example 1.8 *For the tetragonal unit cell of Example 1.1 on page 6, write down the reciprocal components of the lattice vector [114].*

Answer: *This transformation is accomplished by post-multiplication by the direct metric tensor:*

$$t_{[114]}^* = [1 \ 1 \ 4] \begin{bmatrix} \frac{1}{4} & 0 & 0 \\ 0 & \frac{1}{4} & 0 \\ 0 & 0 & 1 \end{bmatrix} = \left[\frac{1}{4} \ \frac{1}{4} \ 4 \right].$$

In other words, the [114] direction is perpendicular to the (1 1 16) plane.

Now we have all the tools we need to express the reciprocal basis vectors in terms of the direct basis vectors. Consider again the vector \mathbf{p} :

$$\mathbf{p} = p_i \mathbf{a}_i.$$

If we replace p_i by $p_m^* g_{mi}^*$, then we have

$$\mathbf{p} = p_m^* g_{mi}^* \mathbf{a}_i = p_m^* \mathbf{a}_m^*,$$

from which we find

$$\mathbf{a}_m^* = g_{mi}^* \mathbf{a}_i, \quad (1.21)$$

and the inverse relation

$$\mathbf{a}_m = g_{mi} \mathbf{a}_i^*. \quad (1.22)$$

In other words, the rows of the metric tensor contain the components of the direct basis vectors in terms of the reciprocal basis vectors, whereas the rows of the reciprocal metric tensor contain the components of the reciprocal basis vectors with respect to the direct basis vectors.

Finally, from equation (1.22) we find after multiplication by the vector \mathbf{a}_k^* :

$$\left. \begin{aligned} \mathbf{a}_m \cdot \mathbf{a}_k^* &= g_{mi} \mathbf{a}_i^* \cdot \mathbf{a}_k^*, \\ \delta_{mk} &= g_{mi} g_{ik}^*. \end{aligned} \right\} \quad (1.23)$$

In other words, the matrices representing the direct and reciprocal metric tensors are each other's inverse. This leads to a simple procedure to determine the reciprocal

basis vectors of a crystal:

- (i) compute the direct metric tensor;
- (ii) invert it to find the reciprocal metric tensor;
- (iii) apply equation (1.21) to find the reciprocal basis vectors.

Example 1.9 *For the tetragonal unit cell of the previous example, write down the explicit expressions for the reciprocal basis vectors. From these expressions, derive the reciprocal lattice parameters.*

Answer: *The components of the reciprocal basis vectors are given by the rows of the reciprocal metric tensor, and thus*

$$\mathbf{a}_1^* = 4\mathbf{a}_1;$$

$$\mathbf{a}_2^* = 4\mathbf{a}_2;$$

$$\mathbf{a}_3^* = \mathbf{a}_3.$$

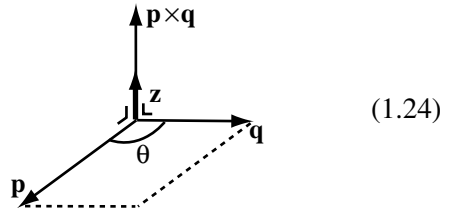
The reciprocal lattice parameters are now easily found from the lengths of the basis vectors: $a^ = |\mathbf{a}_1^*| = |\mathbf{a}_2^*| = 4|\mathbf{a}_1| = 4 \times \frac{1}{2} = 2 \text{ nm}^{-1}$, and $c^* = |\mathbf{a}_3^*| = |\mathbf{a}_3| = 1 \text{ nm}^{-1}$. The angles between the reciprocal basis vectors are all 90° .*

1.3.5 The non-Cartesian vector cross product

The attentive reader may have noticed that we have made use of the *vector cross product* in the definition of the reciprocal lattice vectors, without considering how the cross product is defined in a non-Cartesian reference frame. In this section, we will generalize the cross product to crystallographic reference frames.

Consider the two real-space vectors $\mathbf{p} = p_1\mathbf{a} + p_2\mathbf{b} + p_3\mathbf{c}$ and $\mathbf{q} = q_1\mathbf{a} + q_2\mathbf{b} + q_3\mathbf{c}$. The cross product between them is defined as

$$\mathbf{p} \times \mathbf{q} \equiv \sin \theta |\mathbf{p}| |\mathbf{q}| \mathbf{z},$$



where θ is the angle between \mathbf{p} and \mathbf{q} , and \mathbf{z} is a unit vector perpendicular to both \mathbf{p} and \mathbf{q} . The length of the cross product vector is equal to the area of the parallelogram enclosed by the vectors \mathbf{p} and \mathbf{q} . It is straightforward to compute the components

of the cross product:

$$\begin{aligned}\mathbf{p} \times \mathbf{q} = & p_1 q_1 \mathbf{a} \times \mathbf{a} + p_1 q_2 \mathbf{a} \times \mathbf{b} + p_1 q_3 \mathbf{a} \times \mathbf{c} \\ & + p_2 q_1 \mathbf{b} \times \mathbf{a} + p_2 q_2 \mathbf{b} \times \mathbf{b} + p_2 q_3 \mathbf{b} \times \mathbf{c} \\ & + p_3 q_1 \mathbf{c} \times \mathbf{a} + p_3 q_2 \mathbf{c} \times \mathbf{b} + p_3 q_3 \mathbf{c} \times \mathbf{c}.\end{aligned}$$

Since the cross product of a vector with itself vanishes, and $\mathbf{a} \times \mathbf{b} = -\mathbf{b} \times \mathbf{a}$, we can rewrite this equation as:

$$\begin{aligned}\mathbf{p} \times \mathbf{q} = & (p_1 q_2 - p_2 q_1) \mathbf{a} \times \mathbf{b} + (p_2 q_3 - p_3 q_2) \mathbf{b} \times \mathbf{c} + (p_3 q_1 - p_1 q_3) \mathbf{c} \times \mathbf{a} \\ = & \Omega[(p_2 q_3 - p_3 q_2) \mathbf{a}^* + (p_3 q_1 - p_1 q_3) \mathbf{b}^* + (p_1 q_2 - p_2 q_1) \mathbf{c}^*], \quad (1.25)\end{aligned}$$

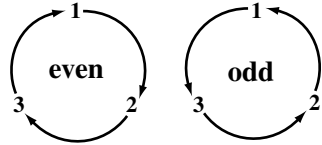
where we have used the definition of the reciprocal basis vectors (equation 1.10). We thus find that the vector cross product between two vectors in direct space is described by a vector expressed in the reciprocal reference frame! This is to be expected since the vector cross product results in a vector perpendicular to the plane formed by the two initial vectors, and we know that the reciprocal reference frame deals with such normals to planes.

In a Cartesian reference frame, the reciprocal basis vectors are identical to the direct basis vectors $\mathbf{e}_i = \mathbf{e}_i^*$ (this follows from equation (1.21) and from the fact that the direct metric tensor is the identity matrix), and the unit cell volume is equal to 1, so the expression for the cross product reduces to the familiar expression:

$$\mathbf{p} \times \mathbf{q} = (p_2 q_3 - p_3 q_2) \mathbf{e}_1 + (p_3 q_1 - p_1 q_3) \mathbf{e}_2 + (p_1 q_2 - p_2 q_1) \mathbf{e}_3.$$

We introduce a new symbol, the *normalized permutation symbol* e_{ijk} . This symbol is defined as follows:

$$e_{ijk} = \begin{cases} +1 & \text{even permutations of 123,} \\ -1 & \text{odd permutations of 123,} \\ 0 & \text{all other cases.} \end{cases}$$



The even permutations of the indices ijk are 123, 231, and 312; the odd permutations are 321, 213, and 132. For all other combinations, the permutation symbol vanishes. The sketch on the right shows an easy way to remember the combinations. We can now rewrite equation (1.25) as

$$\boxed{\mathbf{p} \times \mathbf{q} = \Omega e_{ijk} p_i q_j \mathbf{a}_k^*} \quad (1.26)$$

Note that this is equivalent to the more conventional determinantal notation for the cross product:

$$\mathbf{p} \times \mathbf{q} = \Omega \begin{vmatrix} \mathbf{a}_1^* & \mathbf{a}_2^* & \mathbf{a}_3^* \\ p_1 & p_2 & p_3 \\ q_1 & q_2 & q_3 \end{vmatrix} \left(= \begin{vmatrix} \mathbf{e}_1 & \mathbf{e}_2 & \mathbf{e}_3 \\ p_1 & p_2 & p_3 \\ q_1 & q_2 & q_3 \end{vmatrix} \text{Cartesian} \right).$$

Using equation (1.21), we also find

$$\mathbf{p} \times \mathbf{q} = \Omega e_{ijk} p_i q_j \mathbf{g}_{km}^* \mathbf{a}_m. \quad (1.27)$$

The general definition of the cross product can be used in a variety of situations. A few examples are as follows.

- (i) We can rewrite the definition of the reciprocal basis vectors (1.10) as a single equation, using the permutation symbol:

$$\mathbf{a}_i^* = \frac{1}{2\Omega} e_{ijk} (\mathbf{a}_j \times \mathbf{a}_k), \quad (1.28)$$

where a summation over j and k is implied. From this relation, we can also derive equation (1.21).

- (ii) The volume Ω of the unit cell is given by the mixed product of the three basis vectors:[†]

$$\begin{aligned} \mathbf{a}_1 \cdot (\mathbf{a}_2 \times \mathbf{a}_3) &= \Omega \mathbf{a}_1 \cdot [e_{ijk} \mathbf{a}_{2,i} \mathbf{a}_{3,j} \mathbf{g}_{km}^* \mathbf{a}_m], \\ &= \Omega e_{ijk} \delta_{2i} \delta_{3j} \mathbf{g}_{km}^* \mathbf{a}_1 \cdot \mathbf{a}_m, \\ &= \Omega e_{23k} \mathbf{g}_{km}^* g_{m1}, \\ &= \Omega e_{231} \mathbf{g}_{1m}^* g_{m1}, \\ &= \Omega \delta_{11}, \\ &= \Omega. \end{aligned}$$

Example 1.10 Determine the cross product of the vectors $[110]$ and $[111]$ in the tetragonal lattice of Example 1.1 on page 6.

Answer: From the general expression for the cross product we find

$$\begin{aligned} \mathbf{t}_{[110]} \times \mathbf{t}_{[111]} &= \Omega e_{ijk} \mathbf{t}_{[110],i} \mathbf{t}_{[111],j} \mathbf{a}_k^*, \\ &= \frac{1}{4} [(1 \times 1 - 0 \times 1) \mathbf{a}_1^* + (0 \times 1 - 1 \times 1) \mathbf{a}_2^* + (1 \times 1 - 1 \times 1) \mathbf{a}_3^*], \\ &= \frac{1}{4} (\mathbf{a}_1^* - \mathbf{a}_2^*). \end{aligned}$$

Using the solution for Example 1.9 on page 18, this is also equal to $\mathbf{a}_1 - \mathbf{a}_2$ or the direction vector $[1\bar{1}0]$.

[†] $\mathbf{a}_{i,j}$ is the j th component of the basis vector \mathbf{a}_i , expressed in the direct reference frame \mathbf{a}_i .

It should be intuitively clear that if the cross product of two direct space vectors results in a reciprocal space vector, the reverse should also be true. This is indeed so, and it leads to an important tool for computing the direction indices of a *zone axis*. A zone axis is defined as a direction common to two or more planes. The concept of a zone axis will be crucial for standard electron diffraction techniques, as introduced in Chapter 4.

A direction common to two planes must be perpendicular to both plane normals, and, hence, the direction indices must be proportional to the components of the cross product of the two plane normals. Consider the two planes described by the normals \mathbf{g}_1 and \mathbf{g}_2 . The cross product is given by (by analogy with equation 1.27)

$$\mathbf{g}_1 \times \mathbf{g}_2 = \Omega^* e_{ijk} \mathbf{g}_{1,i} \mathbf{g}_{2,j} g_{km} \mathbf{a}_m^* = \Omega^* e_{ijk} \mathbf{g}_{1,i} \mathbf{g}_{2,j} \mathbf{a}_k.$$

Explicitly working out the summations over i , j , and k we find

$$\mathbf{g}_1 \times \mathbf{g}_2 \parallel (k_1 l_2 - k_2 l_1) \mathbf{a}_1 + (l_1 h_2 - l_2 h_1) \mathbf{a}_2 + (h_1 k_2 - h_2 k_1) \mathbf{a}_3,$$

where we have dropped the reciprocal unit cell volume Ω^* , since direction indices are only defined in terms of relative prime integers.

This leads to a simple practical method for determining the direction indices of a zone axis. First, write down the Miller indices of the two vectors in horizontal rows, as follows:

$$\begin{array}{cccccc} h_1 & k_1 & l_1 & h_1 & k_1 & l_1 \\ h_2 & k_2 & l_2 & h_2 & k_2 & l_2. \end{array}$$

Then remove the first and the last column, i.e.

$$\begin{array}{cccccc} \cancel{h_1} & k_1 & l_1 & h_1 & k_1 & \cancel{l_1} \\ \cancel{h_2} & k_2 & l_2 & h_2 & k_2 & \cancel{l_2}. \end{array}$$

Then compute the three 2×2 determinants formed by the eight remaining numbers above, as in

$$\begin{array}{ccccc} k_1 & & l_1 & & h_1 & & k_1 \\ & \times & & \times & & \times & \\ k_2 & & l_2 & & h_2 & & k_2 \end{array}.$$

This leads to the following components for the direction vector $[uvw]$:

$$\left. \begin{array}{l} u = k_1 l_2 - k_2 l_1; \\ v = l_1 h_2 - l_2 h_1; \\ w = h_1 k_2 - h_2 k_1, \end{array} \right\} \quad (1.29)$$

in agreement with the derivation above. This simple method for the computation of the zone axis indices is rather easy to remember, and it is sufficient for most

computations involving cross products. One should keep in mind, however, that it can only be used if the actual length of the cross product vector is unimportant; i.e. if the resulting indices are rescaled to relative prime integers. If such a rescaling is not allowed, then the general expression (1.27) for the computation of the vector cross product must be used.

Example 1.11 Determine the cross product of the lattice vectors $[110]$ and $[111]$.

Answer: Write the two vectors twice in rows, then remove the first and last columns, and work out the three 2×2 determinants:

$$\begin{vmatrix} \chi & 1 & 0 & 1 & 1 & \emptyset \\ \chi & 1 & 1 & 1 & 1 & \chi \end{vmatrix} = (1\bar{1}0) \quad (= \mathbf{g}_{1\bar{1}0}).$$

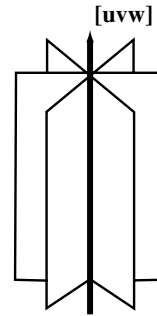
Example 1.12 Determine the cross product of the reciprocal lattice vectors \mathbf{g}_{110} and \mathbf{g}_{111} .

Answer: The answer is identical to that of the previous example, except that the resulting vector is a direct space vector:

$$\begin{vmatrix} \chi & 1 & 0 & 1 & 1 & \emptyset \\ \chi & 1 & 1 & 1 & 1 & \chi \end{vmatrix} = [1\bar{1}0] \quad (= \mathbf{t}_{1\bar{1}0}).$$

Sometimes we will need a general expression for the set of all planes containing a given direction $[uvw]$. Such a collection of planes is known as a *zone*. It is easy to see that a plane belongs to a zone only if its plane normal is perpendicular to the zone axis direction $[uvw]$. This means that the dot product $\mathbf{g}_{(hkl)} \cdot \mathbf{t}_{[uvw]}$ must vanish, or

$$\mathbf{g}_{(hkl)} \cdot \mathbf{t}_{[uvw]} = g_i t_j \mathbf{a}_i^* \cdot \mathbf{a}_j = g_i t_j \delta_{ij} = g_i t_i = 0,$$



or in explicit component notation:

$$\boxed{hu + kv + lw = 0.} \quad (1.30)$$

This equation is known as the *zone equation* and it is valid for all crystal systems.

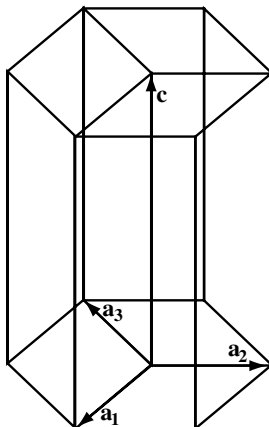


Fig. 1.6. The hexagonal unit cell is not uniquely defined and one can select any of the three cells shown above.

1.4 The hexagonal system

The hexagonal crystal system deserves a separate section because of some subtleties related to the indexing of directions and planes. The lattice parameters for the hexagonal system are given by $\{a, a, c, 90, 90, 120\}$. The choice of the unit cell is not unambiguous, since one can select any one of the three cells indicated in Fig. 1.6. The coplanar vectors \mathbf{a}_i , $i = 1, 2, 3$, and \mathbf{c} form a *linearly dependent* set of four basis vectors. Three non-coplanar basis vectors always suffice for a three-dimensional (3D) crystal, but for the hexagonal system there are advantages to expressing vectors as linear combinations of the four basis vectors.

First of all, we can use the standard (hexagonal) basis vectors \mathbf{a}_1 , \mathbf{a}_2 , and \mathbf{c} to express directions and Miller indices of planes. We will denote the three-index components of a lattice vector \mathbf{t} by the symbol $[u'v'w']$. The Miller indices of a plane with intercepts $\frac{1}{h}, \frac{1}{k}, \frac{1}{l}$ are given by (hkl) , and we can readily define the direct and reciprocal metric tensors for this 3-index system. All equations derived in the previous sections hold for this 3-index description of the hexagonal unit cell.

We can also express directions and plane normals with respect to the four basis vectors \mathbf{a}_1 , \mathbf{a}_2 , \mathbf{a}_3 , and \mathbf{c} . A direction is then specified using the *Miller–Bravais* indices $[uv tw]$, with the third index t referring to the extra basis vector \mathbf{a}_3 , i.e. $\mathbf{t} = u\mathbf{a}_1 + v\mathbf{a}_2 + t\mathbf{a}_3 + w\mathbf{c}$. Similarly, we can define the four-index symbol for a plane by $(hkil)$, with i being proportional to the reciprocal intercept of the plane with the basis vector \mathbf{a}_3 . It is straightforward to show that $i = -(h + k)$, using elementary trigonometry based on Fig. 1.7(a). The 4-index Miller–Bravais system can be described by a 4×4 metric tensor. In the following two sections, we will discuss the subtleties and pitfalls of this 4-index notation.

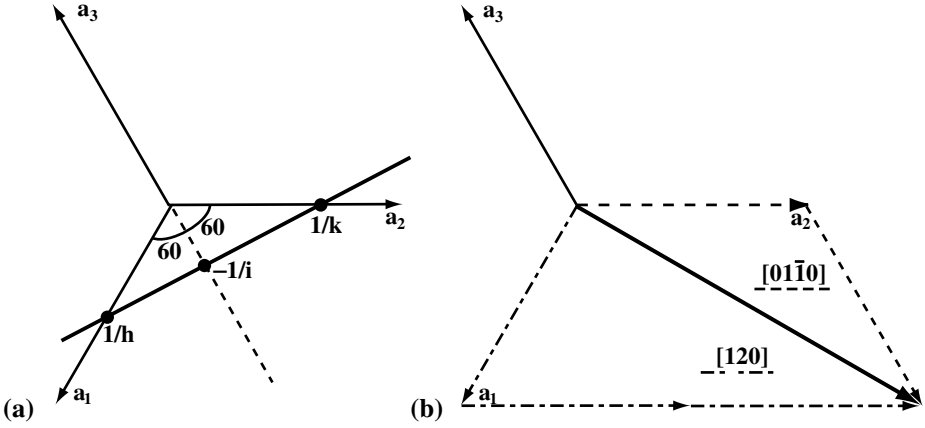


Fig. 1.7. (a) Schematic drawing used to show that $i = -(h + k)$; (b) the $[120] = [01\bar{1}0]$ direction, represented in the 3-index (dash-dotted lines) and 4-index (dashed lines) systems.

1.4.1 Directions in the hexagonal system

We note that the extra basis vector can be written as a linear combination of the other two vectors \mathbf{a}_1 and \mathbf{a}_2 :

$$\mathbf{a}_3 = -(\mathbf{a}_1 + \mathbf{a}_2).$$

There are an infinite number of ways in which a 3D vector can be decomposed with respect to four basis vectors. For simplicity we select the particular decomposition for which $t = -(u + v)$, a relation similar to that for planes (see the next subsection). Let us now determine how this extra index relates to the 3-index notation $[u'v'w']$. The vector \mathbf{t} is given by

$$\mathbf{t} = u'\mathbf{a}_1 + v'\mathbf{a}_2 + w'\mathbf{c} = u\mathbf{a}_1 + v\mathbf{a}_2 + t\mathbf{a}_3 + w\mathbf{c}.$$

Because the vector \mathbf{t} is described by the *sum* of three or four vectors, one cannot simply leave out the third index t to convert from 4-index to 3-index notation. This is allowed for plane normals, as we will see in the next section, but *not* for lattice vectors. The correct transformation relations can easily be shown to be

$$\left. \begin{aligned} u' &= u - t = 2u + v; \\ v' &= v - t = 2v + u; \\ w' &= w. \end{aligned} \right\} \quad (1.31)$$

Table 1.1. *Equivalent indices in the Miller and Miller–Bravais indexing systems for hexagonal directions.*

Miller	Miller–Bravais	Miller	Miller–Bravais
[100]	$[2\bar{1}\bar{1}0]$	[010]	$[\bar{1}2\bar{1}0]$
[110]	$[11\bar{2}0]$	$[\bar{1}10]$	$[\bar{1}100]$
[001]	[0001]	[101]	$[2\bar{1}\bar{1}3]$
[011]	$[\bar{1}2\bar{1}3]$	[111]	$[11\bar{2}3]$
[210]	$[10\bar{1}0]$	[120]	$[01\bar{1}0]$
[211]	$[10\bar{1}1]$	[112]	$[11\bar{2}6]$

The inverse relations are given by

$$\left. \begin{aligned} u &= \frac{1}{3} (2u' - v'); \\ v &= \frac{1}{3} (2v' - u'); \\ t &= -\frac{1}{3} (u' + v') = -(u + v); \\ w &= w'. \end{aligned} \right\} \quad (1.32)$$

The difference between the two indexing systems is illustrated in Fig. 1.7(b): the lattice vector [120] is drawn (dash-dotted lines) as the sum $\mathbf{a}_1 + 2\mathbf{a}_2$, and also (dashed lines) as the sum $\mathbf{a}_2 - \mathbf{a}_3$, corresponding to the 4-index symbol $[01\bar{1}0]$. Table 1.1 lists a few common (low-index) directions in both 3- and 4-index notation.

The metric tensor relations derived in Section 1.2.2, and the equations presented in Tables A1.1–A1.4 are only valid for the 3-index system. To compute the length $|\mathbf{t}|$ of a lattice vector \mathbf{t} in 4-index notation one can proceed in one of two ways:

- first convert the indices to the 3-index system using the relations (1.31) above, then use the standard relations described in this chapter and Table A1.1;
- perform the calculation using the 4-index metric tensor formalism described in the following paragraphs.

Following [OT68], the 4-index metric tensor G is defined in the usual way as

$$G_{ij} \equiv \begin{bmatrix} \mathbf{a}_1 \cdot \mathbf{a}_1 & \mathbf{a}_1 \cdot \mathbf{a}_2 & \mathbf{a}_1 \cdot \mathbf{a}_3 & \mathbf{a}_1 \cdot \mathbf{c} \\ \mathbf{a}_2 \cdot \mathbf{a}_1 & \mathbf{a}_2 \cdot \mathbf{a}_2 & \mathbf{a}_2 \cdot \mathbf{a}_3 & \mathbf{a}_2 \cdot \mathbf{c} \\ \mathbf{a}_3 \cdot \mathbf{a}_1 & \mathbf{a}_3 \cdot \mathbf{a}_2 & \mathbf{a}_3 \cdot \mathbf{a}_3 & \mathbf{a}_3 \cdot \mathbf{c} \\ \mathbf{c} \cdot \mathbf{a}_1 & \mathbf{c} \cdot \mathbf{a}_2 & \mathbf{c} \cdot \mathbf{a}_3 & \mathbf{c} \cdot \mathbf{c} \end{bmatrix} = \frac{a^2}{2} \begin{bmatrix} 2 & -1 & -1 & 0 \\ -1 & 2 & -1 & 0 \\ -1 & -1 & 2 & 0 \\ 0 & 0 & 0 & 2c^2/a^2 \end{bmatrix}. \quad (1.33)$$

The three vectors \mathbf{a}_1 , \mathbf{a}_2 , and \mathbf{a}_3 are coplanar, which means that the determinant of G vanishes. This has important implications for the definition of the reciprocal lattice vectors of the hexagonal system, as described in the next section.

The length of the lattice vector \mathbf{t} in 4-index notation is then derived from the standard equations:

$$|\mathbf{t}|^2 = \mathbf{t} \cdot \mathbf{t} = t_i G_{ij} t_j = \frac{a^2}{2} [u \ v \ t \ w] \begin{bmatrix} 2 & -1 & -1 & 0 \\ -1 & 2 & -1 & 0 \\ -1 & -1 & 2 & 0 \\ 0 & 0 & 0 & 2c^2/a^2 \end{bmatrix} \begin{bmatrix} u \\ v \\ t \\ w \end{bmatrix},$$

from which we can easily derive

$$|\mathbf{t}| = [3a^2 (u^2 + uv + v^2) + c^2 w^2]^{1/2},$$

which is to be compared with the 3-index equation (Table A1.1)

$$|\mathbf{t}| = [a^2 (u'^2 - u'v' + v'^2) + c^2 w'^2]^{1/2}.$$

The angle θ between two lattice vectors in the 4-index notation can also be derived from the G tensor and the result is

$$\cos \theta = \frac{\frac{1}{2}a^2 [6(u_1 u_2 + v_1 v_2) + 3(u_1 v_2 + u_2 v_1)] + c^2 w_1 w_2}{[3a^2 (u_1^2 + u_1 v_1 + v_1^2) + c^2 w_1^2]^{1/2} [3a^2 (u_2^2 + u_2 v_2 + v_2^2) + c^2 w_2^2]^{1/2}}.$$

1.4.2 The reciprocal hexagonal lattice

In Section 1.3.4, we have seen that the reciprocal basis vectors can be written as linear combinations of the direct basis vectors and the rows of the reciprocal metric tensor form the coefficients for this relation. To describe the 4-index reciprocal space, we must first obtain expressions for the reciprocal basis vectors. Since the direct 4-index metric tensor has a zero determinant, its inverse does not exist, so we cannot simply use the same relations to derive the reciprocal basis vectors. Instead we must explicitly derive the reciprocal 4-index basis vectors.

One of the primary motivations for constructing the reciprocal lattice was that triplets of Miller indices (hkl) could then be interpreted as the components of a vector \mathbf{g}_{hkl} . The 4-index notation for the Miller indices $(hkil)$, with $i = -(h + k)$, suggests that there are four reciprocal basis vectors, and that the coefficients h , k , i , and l are the components of the plane normal with respect to those basis vectors. Let us assume, again following [OT68], that there are indeed four basis vectors \mathbf{A}_1^* , \mathbf{A}_2^* , \mathbf{A}_3^* , and \mathbf{C}^* , chosen such that the following relation is valid:

$$\mathbf{g}_{hkl} = h\mathbf{a}_1^* + k\mathbf{a}_2^* + l\mathbf{c}^* = h\mathbf{A}_1^* + k\mathbf{A}_2^* + i\mathbf{A}_3^* + l\mathbf{C}^* = \mathbf{g}_{hkil}. \quad (1.34)$$

In other words, the vector \mathbf{g}_{hkl} is identical to the vector \mathbf{g}_{hkil} , namely the normal to the plane $(hkl) = (hkil) \equiv (hk.l)$. The relation between the 4- and 3-index notation is rather simple: the 3-index notation can be obtained by dropping the third index i from the 4-index symbol. However, we must be careful when interpreting the indices $(hkil)$ as components of a vector! Indeed, from the 3-index reciprocal metric tensor for the hexagonal system follows:

$$\begin{aligned}\mathbf{a}_1^* &= g_{1j}^* \mathbf{a}_j = \frac{4}{3a^2} \mathbf{a}_1 + \frac{2}{3a^2} \mathbf{a}_2; \\ \mathbf{a}_2^* &= g_{2j}^* \mathbf{a}_j = \frac{2}{3a^2} \mathbf{a}_1 + \frac{4}{3a^2} \mathbf{a}_2; \\ \mathbf{c}^* &= g_{3j}^* \mathbf{a}_j = \frac{\mathbf{c}}{c^2}.\end{aligned}$$

After substitution of these relations into equation (1.34), we find for the 4-index reciprocal basis vectors:

$$\begin{aligned}\mathbf{A}_1^* &= \frac{2}{3a^2} \mathbf{a}_1; \\ \mathbf{A}_2^* &= \frac{2}{3a^2} \mathbf{a}_2; \\ \mathbf{A}_3^* &= \frac{2}{3a^2} \mathbf{a}_3; \\ \mathbf{C}^* &= \frac{\mathbf{c}}{c^2}.\end{aligned}$$

It is easy to see that the 4-index reciprocal basis vectors *are not even parallel to the 3-index reciprocal basis vectors!* Instead, they are parallel to the original direct space basis vectors. The relation between the direct basis vectors and the two sets of reciprocal basis vectors is illustrated in Fig. 1.8(a). In Fig. 1.8(b), the $(11\bar{2}0)$ reciprocal lattice point is drawn as two linear combinations: $\mathbf{a}_1^* + \mathbf{a}_2^*$ and $\mathbf{A}_1^* + \mathbf{A}_2^* - 2\mathbf{A}_3^*$. Note that the reciprocal lattice vectors \mathbf{A}_i^* give rise to a reciprocal lattice that is three times as dense as the actual reciprocal lattice; only those points for which $i = -(h + k)$, indicated by larger filled circles in Fig. 1.8(b), should be counted as real reciprocal lattice points.

The 4-index reciprocal metric tensor G^* is then given by

$$G_{ij}^* = \frac{2}{9a^2} \begin{bmatrix} 2 & -1 & -1 & 0 \\ -1 & 2 & -1 & 0 \\ -1 & -1 & 2 & 0 \\ 0 & 0 & 0 & 9a^2/2c^2 \end{bmatrix}. \quad (1.35)$$

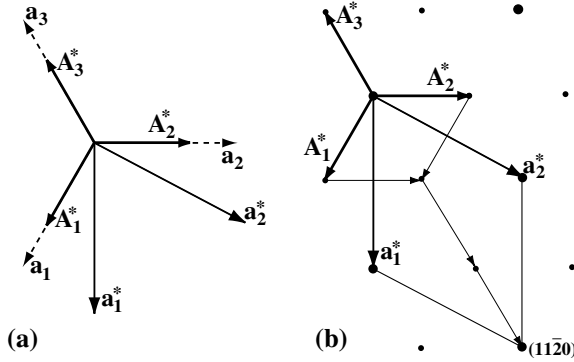


Fig. 1.8. (a) Geometrical representation of the direct and reciprocal basis vectors of the hexagonal lattice; (b) representation of the $(11\bar{2}0)$ reciprocal lattice point.

It is straightforward to show that the length of a reciprocal lattice vector \mathbf{g}_{hkl} is given by

$$|\mathbf{g}_{hkl}| = g_i G_{ij}^* g_j = \frac{4}{9a^2} [h^2 - hk + k^2 - i(h+k) + i^2] + \frac{l^2}{c^2},$$

and after substitution of $i = -(h+k)$, this expression becomes identical to that in Table A1.4. Since the 3- and 4-index equations for $|\mathbf{g}|$ are identical, there is no real need for the G^* reciprocal metric tensor to compute distances and angles in reciprocal space.

Summarizing, the Miller–Bravais and Miller symbols for planes in a hexagonal crystal lattice are related to each other by a simple additional index $i = -(h+k)$; when considered as components of the plane normal, they are expressed with respect to two *different* sets of reciprocal basis vectors. In contrast, the 3- and 4-index expressions for lattice vectors are expressed with respect to the *same* set of basis vectors, but the relation between the sets of indices is somewhat more complex (see equations 1.31 and 1.32). The simultaneous use of 3- and 4-index symbols may cause confusion, so we recommend choosing one of the systems rather than mixing the two systems, in particular when indexing hexagonal diffraction patterns.

As a final note, we point out that the 4-index system, when used as described above, is fully equivalent to the 3-index system and leads to the same type of relations between geometric quantities. As an important example, we mention the *zone equation*, which states when a plane (hkl) belongs to a zone $[uvw]$. In all crystal systems, the zone equation reads as

$$hu + kv + lw = 0.$$

In the 4-index description of the hexagonal system, this equation is still valid, provided the product of the additional indices is added. The dot product of a plane

normal \mathbf{g} with a lattice vector \mathbf{t} in 4-index notation is given by

$$\begin{aligned}\mathbf{t} \cdot \mathbf{g} &= (u\mathbf{a}_1 + v\mathbf{a}_2 + t\mathbf{a}_3 + w\mathbf{c}) \cdot (h\mathbf{A}_1^* + k\mathbf{A}_2^* + i\mathbf{A}_3^* + l\mathbf{C}^*) \\ &= (u\mathbf{a}_1 + v\mathbf{a}_2 + t\mathbf{a}_3 + w\mathbf{c}) \cdot \left(\frac{2h}{3a^2}\mathbf{a}_1 + \frac{2k}{3a^2}\mathbf{a}_2 + \frac{2i}{3a^2}\mathbf{a}_3 + \frac{l}{c^2}\mathbf{c} \right) \\ &= hu + kv + it + lw,\end{aligned}$$

from which the hexagonal 4-index zone equation follows. Throughout this book, we will consistently use the 4-index notation for both directions and planes. The Fortran source code to be discussed in Section 1.9 uses the 3-index notation for all internal computations, but all input–output is performed in the 4-index format.

1.5 The stereographic projection

In this section, we introduce the concept of the *stereographic projection* and describe its importance for electron microscopy. As we shall see in later chapters, conventional TEM observations usually result in two-dimensional (2D) images or diffraction patterns. Since the object giving rise to those images is clearly three-dimensional (3D), we must find a way to represent the crystallographically relevant information in 2D drawings. This section deals with one of the most important 2D representations, the stereographic projection.

A stereographic projection is a 2D representation of a certain characteristic of a 3D object. This characteristic could be the set of normals to the bounding planes (or surfaces) of the object, or the set of directions parallel to all the edges of the object, or some other feature with a *directional* character. The stereographic projection was first proposed in 1839 by William H. Miller [Mil39] as a way to represent the normals to the faces of natural crystals in a 2D drawing, such that direct measurement of the angles between the face normals would be possible from the drawing.

Figure 1.9 shows a sphere of radius R . To obtain the stereographic projection (SP) of a point P on the sphere, we connect the point with the south pole (S) of the sphere and then determine the intersection of this connection line, PS , with the equatorial plane. The resulting point is the stereographic projection of the original point. The point on the sphere could represent the normal to a crystal plane, as shown in the figure, but it could also represent some other direction or directional feature. If the object is oriented such that a symmetry axis coincides with the north–south axis of the projection sphere, then the projection will show a corresponding 2D symmetry. We will discuss crystal symmetries in detail in the next section.

The location of the stereographic projection of a point is most easily computed using spherical coordinates. If the original point has coordinates (R, ϕ, θ) , with ϕ

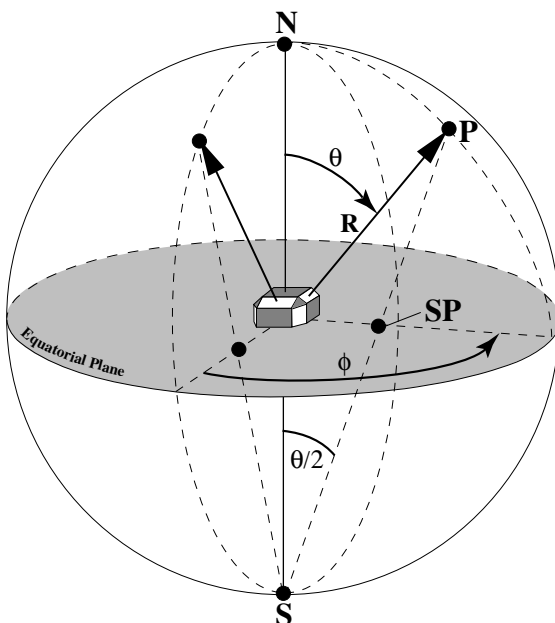


Fig. 1.9. Stereographic projection of the normals on crystal faces.

measured counterclockwise from a fixed axis in the equatorial plane and θ measured from the north pole (z -axis, see Fig. 1.9), then the stereographic coordinates are given by $(\phi, R \tan \frac{\theta}{2})$. From this we see that a point on the equator circle, i.e. with coordinates $(R, \phi, \frac{\pi}{2})$, will have an SP on the equatorial circle with coordinates (ϕ, R) . Points in the southern hemisphere will be projected outside the projection circle; to avoid having to make very large drawings, it is customary to project points in the southern hemisphere from the north pole, and represent the projections with open circles rather than filled circles for projections from the south pole.

The stereographic projection techniques make use of the so-called *Wulff net*, which is shown in Fig. 1.10. A standard Wulff net has a diameter of 20 cm (in the figure this is somewhat reduced to fit on the page). The net shows two sets of arcs: the first set intersects the points M' and M'' and represents the projections of *great circles*; i.e. circles with the same diameter as the projection sphere. If the line $M'-M''$ is taken as the origin for measurement of ϕ , then one can read for each of these great circles the value of θ from the line $A-B$. There is a great circle per degree, and every tenth circle is drawn with a slightly thicker line.

The second set of arcs on the net corresponds to the projection of a set of parallel planes, intersecting the projection sphere in circles. These planes are perpendicular to the equatorial plane and to the $M'-M''$ axis. If the projection sphere is rotated

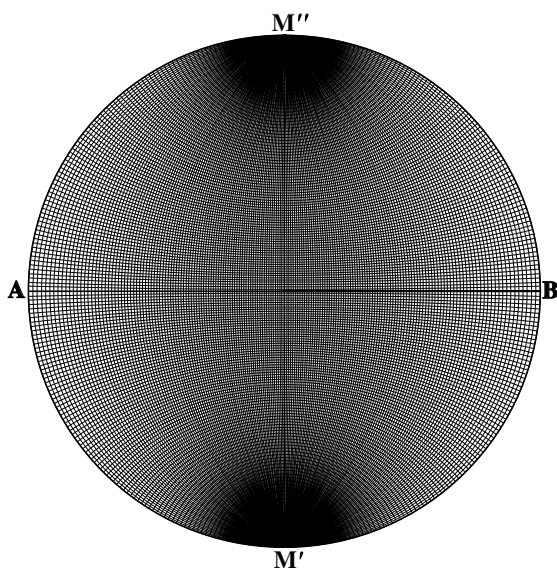


Fig. 1.10. Standard Wulff net for stereographic projections.

around this axis, then a point on the surface will trace a circular path; the projection of this path is given by the second set of arcs, which are again spaced by 1° .

Stereographic projections conserve angles; i.e. measurement of an angle on the projection will always correspond to the real 3D angle. It is this property that turns the SP into a rather useful technique for crystallography and TEM. In the following paragraphs, we will discuss several basic (manual) operations using the Wulff net. Some computer programs have all of these routines available, but it is often useful to know how to do them by hand.

The Wulff net is commercially available from various manufacturers (see website); one could also make a simple Wulff net using the PostScript file `wulff.ps` available from the website. The easiest way to use the net is to print or glue it on a thick piece of paper, and cut around the circle, leaving about 10 mm of extra space all around the edge. Figure 1.11 then shows how the net can be used to produce manual stereographic projections. A transparency is mounted with pins or tape onto a board. The Wulff net is then positioned underneath the transparency, such that the entire projection circle is covered by it. Then a pin is inserted through both the transparency and the Wulff net (through the center of the net), such that the whole assembly is firmly attached to the board. The Wulff net can then be turned around the pin, while the transparency remains fixed. All of the following sections assume that the reader has a similar setup available for manual stereographic projections.

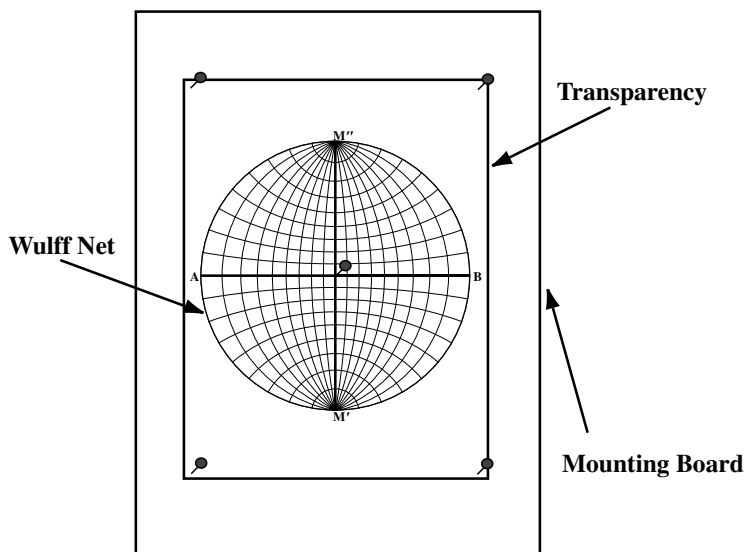


Fig. 1.11. Illustration of the manual use of a Wulff net for stereographic projections.

1.5.1 Drawing a point

Drawing a single point is the most elementary operation one can perform on a stereographic net. Let us assume that the standard net is being used, and that the 3D spherical coordinates of a point are known. They can be transferred onto the net in the following way: align the line $A-B$ (by rotating the net) such that it is parallel to the bottom of the transparency. Then draw the line $A-B$ onto the transparency; this will be your reference line and we will call it $R-S$ (see Fig. 1.12a). If the coordinates of the point are (R, ϕ, θ) , rotate the net over an angle ϕ (such that the line $A-B$ on the net makes an angle ϕ with $R-S$). From the point M'' , measure the angle θ along the outer circle;[†] connect the corresponding point with the point M' . The intersection of this line with the line $A-B$ (the point p) is the SP of the original point.

1.5.2 Constructing a great circle through two poles

If two points p and q are known (Fig. 1.12b), then the great circle through those points can easily be found as follows: we know that the arcs connecting the points M' and M'' are projections of great circles. Therefore, we rotate the net until one of those arcs connects the two points. The resulting arc is then the projection of the great circle through the two given points.

[†] Alternatively one could measure the angle θ from the center of the circle along the line $A-B$.

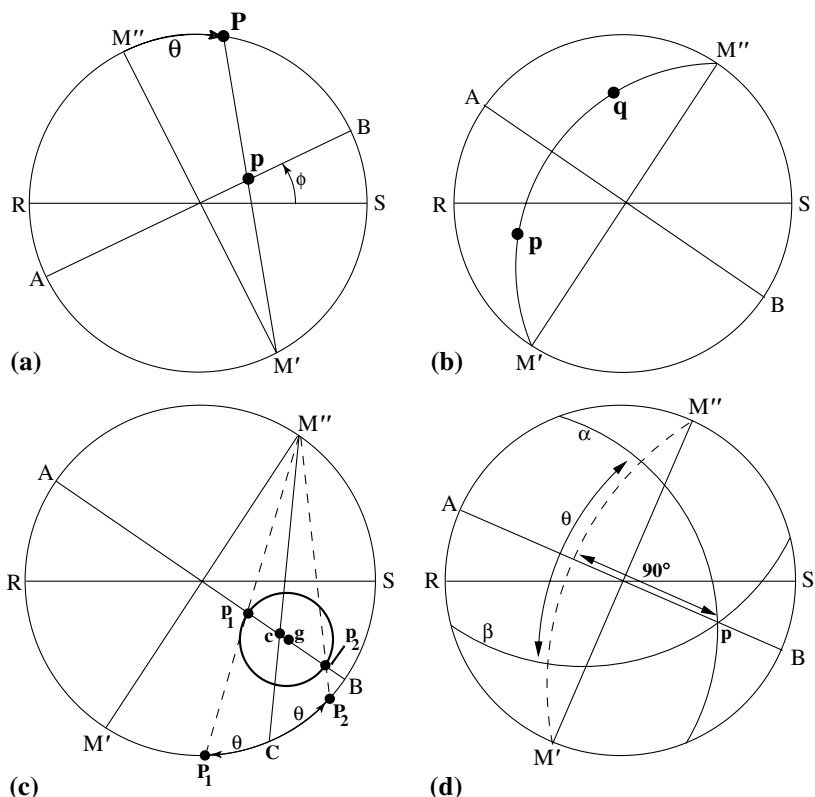


Fig. 1.12. (a) Determination of the SP of a single point, the spherical coordinates of which are known; (b) determination of the great circle through two points; (c) drawing a circle of radius θ around a point c ; (d) determination of the angle between two great circles.

1.5.3 Constructing a small circle around a pole

We now wish to draw a circle with radius θ around a given pole. One general and two trivial solutions exist. If the center of the circle, i.e. the given pole, coincides with the center of the projection, then the circle can easily be drawn by reading the radius θ along the line $A-B$ and using a compass set to this radius. If the circle has its pole on the equatorial plane, then all we need to do is rotate the net such that the point M' coincides with the pole; circles centered on M' are already drawn on the net and we only need to copy the one corresponding to θ .

The general case, where the pole does not lie in the center or on the equator, is shown in Fig. 1.12(c). Suppose the given pole is indicated by the point c . The center of the projection of a circle will, in general, not coincide with the projection of the center of the circle. The projected center can be found as follows: bring the line $A-B$ onto the point c . From the point M'' , draw a line through c which intersects the outer circle in C . Measure the angle θ on both sides of C , along the

outer circle. Connect the resulting points P_1 and P_2 with M'' . The intersections of these lines with the line $A-B$ are called p_1 and p_2 ; both of these points lie on the projected circle. The center g of the projected circle lies midway between p_1 and p_2 and has radius gp_1 . This completes the construction. The construction of circles is useful for error bars and for some aspects of trace analysis.

1.5.4 Finding the pole of a great circle

The pole of a great circle is defined as the north pole for that circle; i.e. it lies 90° away from each point of the circle. Since great circles on the Wulff net connect the points M' and M'' , the corresponding pole can be found by measuring 90° along the line $A-B$ from the intersection point of the great circle and this line. This construction is used to determine the location of a zone axis when two points of the zone are known.

1.5.5 Measuring the angle between two poles

Since the SP conserves angles, one can easily determine angles from the projection diagram. If two points, p and q , are known, one can draw the great circle through these points (see above) and then read the angle along that great circle from the Wulff net.

1.5.6 Measuring the angle between two great circles

The angle between two great circles is also easily determined: if the great circles α and β are given (Fig. 1.12d), bring the line $A-B$ through their intersection point p , measure 90° along that line, and draw the great circle corresponding to the pole p . The angle between the intersections of this circle with the circles α and β is the required angle. We will use the various methods introduced in this section when we discuss trace analysis in Chapter 8.

1.6 Crystal symmetry




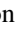
An object is said to have a certain symmetry if any operations exist which leave this object *invariant*. A symmetry operation is, thus, a mathematical operation that leaves the distances between all material points of an object unchanged (i.e. no stretching, twisting, shearing, or bending) or, equivalently, a symmetry operation is an *isometric* operation. The symmetry operations relevant for crystallography are translations, rotations, reflections, inversions, and their combinations. Only a

finite number of combinations of such symmetry operations are compatible with the 14 Bravais lattices. The 230 allowed (and unique) combinations of symmetry elements are known as the three-dimensional (3D) *space groups*, and they are tabulated in [Hah96]. In this section, we will describe, with minimal derivations, those aspects of symmetry theory of importance for electron microscopy. In particular, we will describe the mathematical representation of symmetry operators, the 32 point groups, the 230 space groups, and how they can be used.

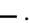
1.6.1 Symmetry operators

We distinguish between two basic kinds of symmetry operations: those that can be physically realized (rotations and translations), also known as operations of the first kind, or *proper operations*, and those that change the *handedness* of an object (reflection and inversion), operations of the second kind. All symmetry operations are represented by unique graphical symbols.

Operations of the first kind

- (i) A pure rotation is characterized by a rotation axis $[uvw]$ and a rotation angle $\alpha = 2\pi/n$. The integer n is the *order* of the rotation and we say that a rotation is n -fold if its angle is given by $2\pi/n$. A pure rotation of order n is denoted by the symbol **n**. This is the so-called International or Hermann–Mauguin notation.[†] In drawings an n -fold rotation axis is represented by a filled regular polygon with n sides. A six-fold rotation axis perpendicular to the drawing plane is then indicated by the  symbol, a four-fold axis by , a three-fold axis by , and a two-fold axis by .
- (ii) A pure translation is characterized by a translation vector **t**. We have already discussed translations earlier in this chapter. In drawings, translation vectors are indicated by arrowed lines.

Operations of the second kind

- (i) A *pure reflection* is characterized by a plane (hkl), and the International symbol for a mirror plane is **m**. The Schönflies symbol is the Greek letter σ . In a drawing a mirror plane is always indicated by a thick solid line, .
- (ii) An *inversion* is a point symmetry operation that takes all the points **r** of an object and projects them onto $-\mathbf{r}$. The operation is usually denoted by $\bar{1}$ or sometimes by i . In drawings the inversion center is denoted by the symbol \circ (i.e. a small open circle).

Symmetry operations are often represented by means of stereographic projections. Figure 1.13 shows the stereographic projections for a three-fold rotation, a

[†] There is a second notation system, the *Schönflies* system, in which rotations are indicated by the symbol C_n . Even though the International system is the preferred system, we will also mention the Schönflies notation because it is still frequently used.

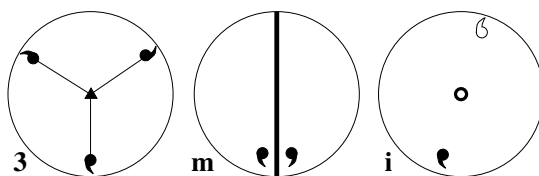


Fig. 1.13. Stereographic representation of a three-fold rotation, a mirror plane perpendicular to the projection plane, and an inversion.

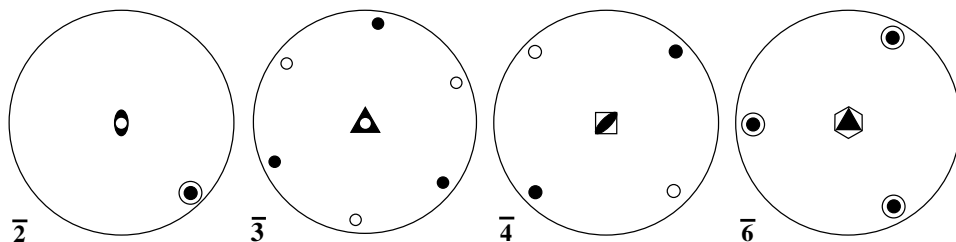


Fig. 1.14. Stereographic representation of the crystallographic rotoinversions.

mirror plane perpendicular to the projection plane, and an inversion. Note that the object does not have any symmetry itself (a circle with a curved tail), so that a change in handedness is readily observed.

The basic symmetry operations of the first and second kind can be combined with each other to create new symmetry operations. There are three combinations of interest to crystallography:

- combination of rotations with the inversion center;
- combination of rotations with translations;
- combination of mirrors with translations.

1.6.1.1 Combination of a rotation with the inversion center

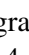
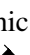
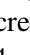
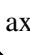
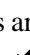
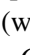
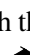
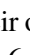
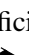
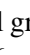

The combination of a rotation axis with an inversion center located somewhere on that axis is called a *rotoinversion operation*. The rotoinversion rotates a point over an angle $2\pi/n$ **and** inverts the resulting point through the inversion center. A rotoinversion of order one is equivalent to the inversion operation i . Rotoinversions are represented by the symbol \bar{n} and the crystallographic rotoinversions are shown in the stereographic projections of Fig. 1.14. They are represented by special symbols: $\bar{2}$ for $\bar{2}$, $\bar{3}$ for $\bar{3}$, $\bar{4}$ for $\bar{4}$, and $\bar{6}$ for $\bar{6}$.

1.6.1.2 Combination of a rotation with a translation

For all symmetry operations except the translation, repeated operation eventually returns one to the initial point; e.g. three subsequent operations of the three-fold

axis \blacktriangle complete a 360° rotation, and two subsequent mirror operations reproduce the original object again. For combinations of symmetry elements involving the translation, this is no longer the case and one never returns to the initial point, no matter how many times the operation is repeated.

A *screw axis* \mathbf{n}_m consists of a counterclockwise rotation through $2\pi/n$ followed by a translation $\mathbf{T} = \frac{m}{n} \mathbf{t}_{[uvw]}$ in the positive direction $[uvw]$ along the screw axis. The vector \mathbf{T} is known as the *pitch* of the screw axis. Screw axes of the type \mathbf{n}_m and \mathbf{n}_{n-m} are mirror images of each other. A screw axis is called *right-handed* if $m < n/2$, *left-handed* if $m > n/2$, and *without hand* if $m = 0$ or $m = n/2$. Screw axes related to each other by a mirror operation are called *enantiomorphous*.

The crystallographic screw axes are (with their official graphical symbols): 2_1 , 3_1 , 3_2 , 4_1 , 4_2 , 4_3 , 6_1 , 6_2 , 6_3 , 6_4 , and 6_5 . All screw axes are shown in Fig. 1.15: the number next to each circle refers to the height of the circle above the plane of the drawing. The axes are all perpendicular to the drawing.

1.6.1.3 Combination of a mirror plane with a translation

The last class of symmetry operators involves combinations of mirror planes and translations. We define the *glide plane* as the combined operation of a mirror with

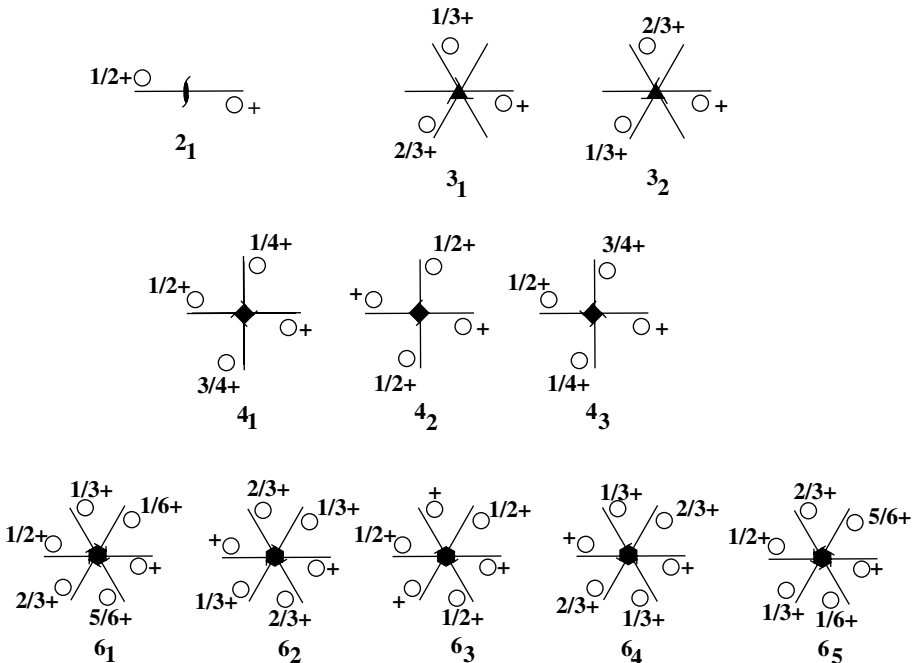


Fig. 1.15. Schematic representation of all crystallographic screw axes.

Table 1.2. Different types of mirror and glide planes, their symbols and glide vectors.

Name	Symbol	Glide vectors
Mirror	m	None
Axial glide	a	$\frac{a}{2}$
	b	$\frac{b}{2}$
	c	$\frac{c}{2}$
Diagonal glide	n	$\frac{a+b}{2}, \frac{b+c}{2}, \frac{c+a}{2}, \frac{a+b+c}{2}^\dagger$
Diamond glide	d	$\frac{a+b}{4}, \frac{b+c}{4}, \frac{c+a}{4}, \frac{a+b+c}{4}^\dagger$

[†]These glide vectors are only possible in cubic and tetragonal systems.

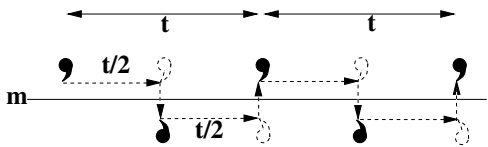


Fig. 1.16. Schematic representation of a glide plane.

a translation over *half* a lattice vector parallel to the mirror plane. An example is shown in Fig. 1.16.

The allowed glide vectors must be equal to one-half of the lattice vectors; in the case of centered Bravais lattices there are additional glide vectors, equal to one-half of the centering vectors $\frac{1}{2}(\mathbf{a} + \mathbf{b})$, $\frac{1}{2}(\mathbf{b} + \mathbf{c})$, $\frac{1}{2}(\mathbf{c} + \mathbf{a})$, and $\frac{1}{2}(\mathbf{a} + \mathbf{b} + \mathbf{c})$. Table 1.2 lists the various possibilities and names for all types of glide planes.

The official drawing symbols for glide planes depend on the orientation of the plane with respect to the drawing. If the plane is perpendicular to the drawing, then the plane is indicated by a solid bold line for m , a dashed bold line for a glide with translation in the plane of the drawing, a dotted bold line for a glide with translation perpendicular to the plane of the drawing, and a dash-dotted bold line for a diagonal glide (see Fig. 1.17). Note that a circle reflected in a mirror plane is represented by a circle with a comma in the center, indicating that an odd number of reflections relate that point to the original point. For glide planes parallel to the plane of the drawing, one uses a symbol based on \neg , which represents a pure mirror. For an axial glide plane, an arrow is added to the symbol in the direction of the glide vector, i.e. $\neg\rightarrow$. For a diagonal glide, the arrow points at an angle away from the corner, as in $\neg\swarrow$. Examples are shown in the right-hand column of Fig. 1.17.

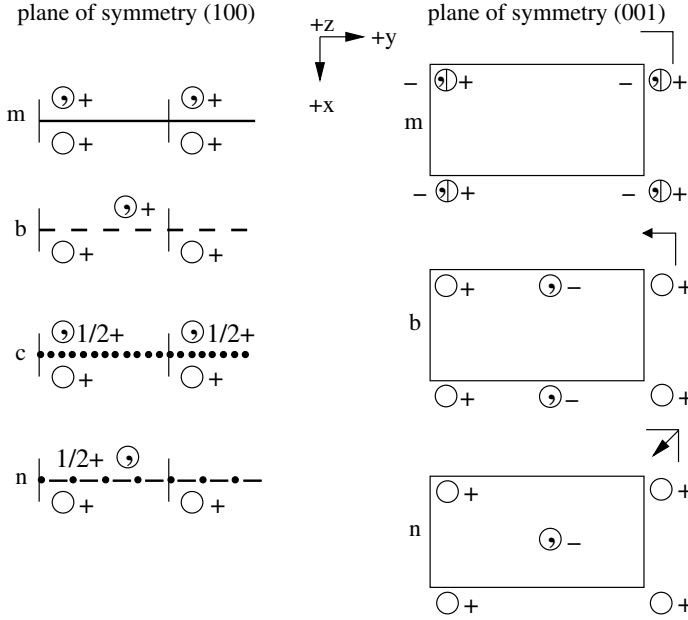


Fig. 1.17. Graphical representation of glide planes perpendicular (left) and parallel (right) to the plane of the drawing. (Figure based on Fig. 4.16 in [MM86].)

1.6.2 Mathematical representation of symmetry operators

A symmetry operator \mathcal{O} operating on a material point \mathbf{r} transforms its coordinates into a new vector \mathbf{r}' with components (x'_1, x'_2, x'_3) as follows:

$$\mathbf{r}' = \mathcal{O}[\mathbf{r}]. \quad (1.36)$$

In the previous section we saw that the most general crystallographic symmetry operator \mathcal{O} consists of a rotation/inversion/reflection and, sometimes, a translation. This means that in mathematical terms the coordinates of the new point can be derived from those of the old point by first applying the rotation/inversion/reflection and then adding the translation vector. This is explicitly described by

$$\begin{aligned} x'_1 &= D_{11}x_1 + D_{12}x_2 + D_{13}x_3 + u_1; \\ x'_2 &= D_{21}x_1 + D_{22}x_2 + D_{23}x_3 + u_2; \\ x'_3 &= D_{31}x_1 + D_{32}x_2 + D_{33}x_3 + u_3. \end{aligned}$$

Using the *Einstein summation convention* this set of equations can be rewritten as

$$x'_i = D_{ij}x_j + u_i, \quad (1.37)$$

or, in operator form,

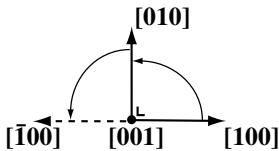
$$\mathbf{r}' = \mathbf{D}\mathbf{r} + \mathbf{t} = (\mathbf{D}|\mathbf{t})[\mathbf{r}] = \mathcal{O}[\mathbf{r}]. \quad (1.38)$$

The matrix \mathbf{D} describes the *point symmetry transformation* and the vector \mathbf{t} describes the translational component of the operator \mathcal{O} . In the crystallographic literature, the point symmetry part is usually called the *linear part* and the whole operator is called a *motion*. The compact notation $(\mathbf{D}|\mathbf{t})$ is called the *Seitz symbol*.

The symmetry matrices can be defined with respect to a generic Cartesian reference frame, or with respect to the Bravais lattice vectors \mathbf{a}_i . The latter choice is the most convenient one, and it is straightforward to determine the entries of the matrix D_{ij} for any given symmetry operation. All that is needed are the transformations of the basis vectors $[100]$, $[010]$, and $[001]$. The columns of the matrix D_{ij} then contain the components of the new points; i.e. the components of the point $\mathcal{O}([100])$ are given by the column D_{i1} , $\mathcal{O}([010])$ is given by D_{i2} and so on. An example will illustrate the procedure.

Example 1.13 Determine the transformation matrix D_{ij} for the operator **4**, parallel to the \mathbf{a}_3 direction of a tetragonal unit cell.

Answer: From the drawing below one can determine readily that the operator rotates the $[100]$ vector onto the vector $[010]$, $[010]$ is rotated onto the vector $[\bar{1}00]$, and the vector $[001]$ is invariant since it lies on the rotation axis. The columns of the matrix are then formed by the vectors $[010]$, $[\bar{1}00]$, and $[001]$, or[†]

$$D_{ij} = \begin{pmatrix} 0 & -1 & 0 \\ 1 & 0 & 0 \\ 0 & 0 & 1 \end{pmatrix}.$$


For computational purposes, it is convenient to work with four-dimensional vectors instead of the regular three-dimensional vectors. This sounds complicated, but it is really very simple: to each triplet of vector components (x_1, x_2, x_3) we simply add the number 1 as the fourth component, i.e. $(x_1, x_2, x_3, 1)$. This type of coordinate is called a *normal coordinate*. The fourth component must always be equal to 1, and is denoted by x_4 .

[†] We will use the convention that a regular matrix is surrounded by parentheses, whereas a matrix representing a tensor will be denoted by square brackets.


The reason for the introduction of normal coordinates is the following: let us define a 4×4 -matrix \mathcal{W} of the following form:

$$\mathcal{W} = \begin{pmatrix} D_{11} & D_{12} & D_{13} & u_1 \\ D_{21} & D_{22} & D_{23} & u_2 \\ D_{31} & D_{32} & D_{33} & u_3 \\ 0 & 0 & 0 & 1 \end{pmatrix}. \quad (1.39)$$

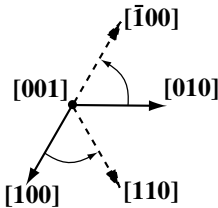
In other words, \mathcal{W} contains the matrix \mathbf{D} and the translation vector \mathbf{t} . If we denote a four-dimensional vector by the symbol $\bar{\mathbf{r}} = (x_1, x_2, x_3, 1)$, then the equation

$$\bar{\mathbf{r}}' = \mathcal{W}\bar{\mathbf{r}}$$

fully describes the symmetry operation, as can be verified easily by writing out the component equations.

Example 1.14 Determine the matrix \mathcal{W} for a  screw axis parallel to the \mathbf{a}_3 axis of a hexagonal unit cell.

Answer: This screw axis of order six has a 60° rotation combined with a pitch vector $\mathbf{T} = \frac{1}{6}\mathbf{a}_3$. As can be verified from the drawing below we have the following transformations of the basis vectors: $\mathcal{O}([100]) = [110]$, $\mathcal{O}([010]) = [\bar{1}00]$, and $[001]$ is invariant. The matrix \mathcal{W} is therefore given by

$$\mathcal{W} = \begin{pmatrix} 1 & \bar{1} & 0 & 0 \\ 1 & 0 & 0 & 0 \\ 0 & 0 & 1 & \frac{1}{6} \\ 0 & 0 & 0 & 1 \end{pmatrix}.$$


The main advantage of expressing the transformation matrices in terms of the basis vector of the Bravais lattice is that the components of the matrix D_{ij} are always simple integers (-1 , 0 , or 1). The 60° rotation of Example 1.14 would have the numbers $\frac{1}{2}$ and $\pm\sqrt{3}/2$ as entries in the transformation matrix if the operator were expressed with respect to a standard Cartesian reference frame. The translational part of the matrix \mathcal{W} may, of course, contain fractions or integer numbers. This will become important when we implement space groups in a computer program (see Section 1.9.3).

Table 1.3. *Multiplication table for the three-fold rotation group $\mathbf{3}$.*

	\mathcal{E}	$\mathbf{3}$	$\mathbf{3}^2$
\mathcal{E}	\mathcal{E}	$\mathbf{3}$	$\mathbf{3}^2$
$\mathbf{3}$	$\mathbf{3}$	$\mathbf{3}^2$	\mathcal{E}
$\mathbf{3}^2$	$\mathbf{3}^2$	\mathcal{E}	$\mathbf{3}$

1.6.3 Point groups

Group theory plays an important role in crystallography because it allows for a systematic description of all possible crystal symmetries, and consequently, all crystal structures. The central concept in group theory is that of a *group*. A group is a set \mathcal{G} of elements \mathcal{O}_i , $i = 1, \dots, N$, where N may be finite or infinite. If a multiplication operation is defined by writing two elements of the set next to each other, i.e. $\mathcal{O}_i\mathcal{O}_j$ (meaning that the operation \mathcal{O}_j is performed first, followed by \mathcal{O}_i), then the set \mathcal{G} is a group if the following four conditions are satisfied:

- (i) every product $\mathcal{O}_i\mathcal{O}_j$ belongs to the set \mathcal{G} (the set is *closed* under the multiplication);
- (ii) for every three elements we have $\mathcal{O}_i(\mathcal{O}_j\mathcal{O}_k) = (\mathcal{O}_i\mathcal{O}_j)\mathcal{O}_k$ (the multiplication is *associative*);
- (iii) there exists an *identity element* \mathcal{E} , such that $\mathcal{E}\mathcal{O}_i = \mathcal{O}_i\mathcal{E} = \mathcal{O}_i$ for every operator \mathcal{O}_i ;
- (iv) and every element \mathcal{O}_i has an *inverse element* \mathcal{O}_k , such that $\mathcal{O}_i\mathcal{O}_k = \mathcal{O}_k\mathcal{O}_i = \mathcal{E}$.

If, in addition, the product of *any* pair of elements is independent of the order of multiplication, then the group is said to be *Abelian* or *commutative*.

A simple example of a finite group is the set consisting of the identity element and a three-fold rotation axis $\mathbf{3}$; there are three elements in the set, \mathcal{E} , $\mathbf{3}$, and $\mathbf{3}^2$ (i.e. a rotation over $240^\circ = -120^\circ$). It is straightforward to verify that this set satisfies all five conditions above, so that the set $\{\mathcal{E}, \mathbf{3}, \mathbf{3}^2\}$ is an Abelian group. A standard tool for verifying whether or not a set is a group is the *multiplication table* (also known as *Cayley's square*). The multiplication table for the three-fold rotation group is shown in Table 1.3. If every element of the set occurs once in each row and once in each column, then the set is a group. If, in addition, the table is symmetric with respect to the main diagonal, then the group is an Abelian group. There are many examples of infinite groups. The simplest one is perhaps the set of integer numbers, which, as is easily checked, forms an infinite Abelian group under the addition operation.

Before considering the application of group theory to crystallography we must determine which symmetry operations are possible in crystals. One can easily

Table 1.4. Allowed angles between rotation axes of orders A , B , and C , compatible with the Bravais lattices.

A	B	C	$\hat{B}\hat{C}$	$\hat{A}\hat{C}$	$\hat{A}\hat{B}$
2	2	2	90°	90°	90°
2	2	3	90°	90°	60°
2	2	4	90°	90°	45°
2	2	6	90°	90°	30°
2	3	3	$70^\circ 32'$	$54^\circ 44'$	$54^\circ 44'$
2	3	4	$54^\circ 44'$	45°	$35^\circ 16'$

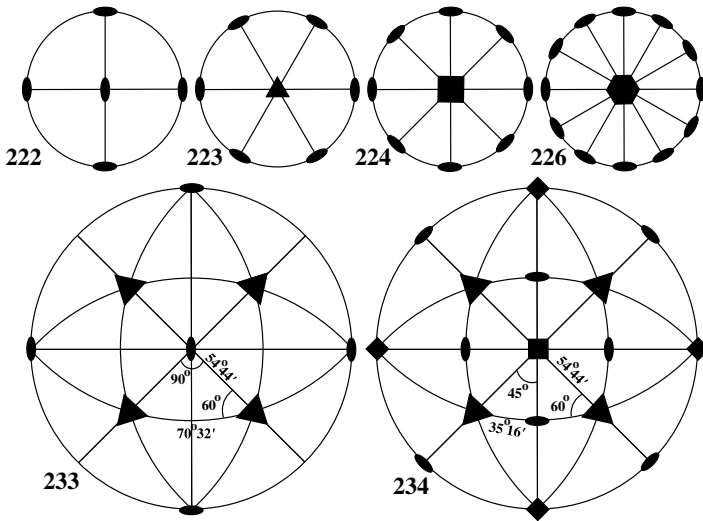


Fig. 1.18. Stereographic projections of the six crystallographically allowed combinations of rotational axes.

show that the only rotational symmetry operations compatible with the translational periodicity of the Bravais lattices are the rotations of order 1, 2, 3, 4 and 6 (e.g. [MM86]). Furthermore, only six combinations of multiple rotation axes are possible in any given Bravais lattice[†]: 222, 223, 224, 226, 233, and 234. The angles between those rotation axes are fixed and given in Table 1.4. Stereographic projections of these combinations of rotation elements are shown in Fig. 1.18.

When the simple rotational symmetries 1, 2, 3, 4, and 6, and the six combinations in Fig. 1.18 are combined with all possible combinations of mirror planes and the inversion symmetry, 32 distinct crystallographic point symmetries are found (they

[†] For an explicit derivation of these statements we refer the interested reader to [MM86] or [BG90].

Table 1.5. **International**–[Schœnflies] notation, group order N and crystal system S (a , m , h , R , o , t or c) for the 32 crystallographic point groups.

Point group	N	S	Point group	N	S
1 –[C_1]	1	a	$\bar{3}$ –[S_6]	6	R
$\bar{1}$ –[C_i]	2	a	32 –[D_3]	6	R
2 –[C_2]	2	m	3m –[C_{3v}]	6	R
m –[C_s]	2	m	$\bar{3}m$ –[D_{3d}]	12	R
2/m –[C_{2h}]	4	m	6 –[C_6]	6	h
222 –[D_2]	4	o	$\bar{6}$ –[C_{3h}]	6	h
mm2 –[C_{2v}]	4	o	6/m –[C_{6h}]	12	h
mmm –[D_{2h}]	8	o	622 –[D_6]	12	h
4 –[C_4]	4	t	6mm –[C_{6v}]	12	h
$\bar{4}$ –[S_4]	4	t	$\bar{6}m2$ –[D_{3h}]	12	h
4/m –[C_{4h}]	8	t	6/mmm –[D_{6h}]	24	h
422 –[D_4]	8	t	23 –[T]	12	c
4mm –[C_{4v}]	8	t	m3 –[T_h]	24	c
$\bar{4}2m$ –[D_{2d}]	8	t	432 –[O]	24	c
4/mmm –[D_{4h}]	16	t	$\bar{4}3m$ –[T_d]	24	c
3 –[C_3]	3	R	m$\bar{3}m$ –[O_h]	48	c

are called *point symmetries* because all symmetry elements intersect each other at one point). These 32 combinations are known as the 32 *point groups*. Their names in both International (Hermann–Mauguin) notation and Schœnflies notation, number of elements (order), and corresponding crystal systems are listed in Table 1.5. Stereographic projections can be found in Appendix A4, together with rendered drawings of the point group symmetry elements. Detailed drawings for all point groups, as well as Quicktime, AVI, and animated GIF movies illustrating the 3D structure of each point group are available from the website. Examples of rendered drawings for the point groups **4/m** and **m $\bar{3}m$** are shown in Fig. 1.19; the general position in the point group is represented by a right-handed helix and it can be seen that the rotation axis preserves the handedness, whereas the mirror plane reverses the handedness of the helices. The handedness of the general point is not usually represented in stereographic projections of the point groups (such as those shown in Appendix A4).

1.6.4 Families of planes and directions

In a given crystal system the set of directions equivalent to $\mathbf{t} = [uvw]$ is given by

$$t_i (D^{(k)}) = D_{ij}^{(k)} t_j \quad k = 1, \dots, N, \quad (1.40)$$

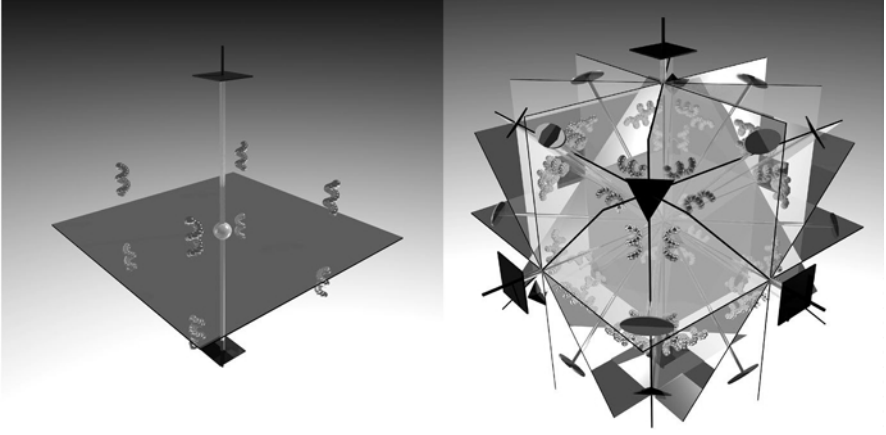


Fig. 1.19. Rendered images of the point groups $4/m$ and $m\bar{3}m$. The general point is represented by a short helix, so that the action of the operators of the second kind is properly shown. Details about how this image and those in Appendix A4 were created can be found in [DG98] and on the website.

where the N matrices $D^{(k)}$ are the point symmetry matrices of the corresponding *point group*. The set of equivalent directions is known as a *family*, and is denoted by the symbol $\langle uvw \rangle$. Note that the number of members in a family depends on the point symmetry of the crystal.

Since the symmetry matrices $D^{(k)}$ are defined with respect to the direct basis vectors, we cannot always use the same matrices to determine the set of reciprocal lattice vectors equivalent to \mathbf{g}_{hkl} . Both the symmetry matrix and the reciprocal lattice vector must be expressed *in the same reference frame* before the equivalent vectors can be determined. This means that we must transform the reciprocal lattice vector \mathbf{g}_{hkl} to direct space, compute the equivalent vectors using the set of N matrices $D^{(k)}$, and then transform all equivalent vectors back to reciprocal space. This is expressed mathematically by

$$g_m(D^{(k)}) = g_{ml} D_{lj}^{(k)} g_{ji}^*. \quad (1.41)$$

Alternatively, we can first compute the components of the symmetry matrices in reciprocal space, resulting in a set of N matrices $D^{*(k)}$, and then operate with these matrices on the reciprocal lattice vector \mathbf{g}_{hkl} . The set of reciprocal symmetry matrices is given by

$$D_{mi}^{*(k)} = g_{ml} D_{lj}^{(k)} g_{ji}^*. \quad (1.42)$$

The set of plane normals equivalent to (hkl) is denoted by the family $\{hkl\}$; the number of members again depends on the point symmetry of the crystal.

The concept of *family* is used whenever the components of the vectors are all integers (as in $[uvw]$ or (hkl)). For non-integer components one can define similar concepts: the set of points $\mathbf{r}^{(k)}$ equivalent to a given general point \mathbf{r} is known as the *orbit* of \mathbf{r} . In reciprocal space the set of points $\mathbf{q}^{(k)}$ equivalent to \mathbf{q} is known as the *star* of \mathbf{q} . The number of members in a family, orbit, or star is generally known as its *multiplicity*. In Section 1.9 we will discuss a method to determine numerically the point symmetry matrices of an arbitrary point group, based on the space group symmetry.

1.6.5 Space groups

The point groups enumerate all combinations of symmetry elements consistent with the translational symmetry of the Bravais lattices. They describe the symmetry of an object with respect to a single fixed point. When the point group symmetries are combined with the translational symmetry operators of the Bravais lattices, one can show that there are precisely 230 unique combinations. This was shown independently by Fedorov in Russia [Fed90], Schœnflies in Germany [Sch91], and Barlow in England [Bar94] during the last decade of the 19th century. This is a rather important finding because it means that every crystal structure must belong to one of those 230 symmetries. Since a combination of a point group and a Bravais lattice creates an infinite lattice, the resulting symmetry groups (of infinite order) are known as *space groups*.

The simplest space groups can be constructed by selecting one of the point groups and one of the Bravais lattices for the corresponding crystal system, and copying the symmetry elements of the point group onto every lattice site of that Bravais lattice. In this way, one can construct 73 different combinations, known as the *symmorphic space groups*. A table with all 73 symmorphic space groups is reproduced in Appendix A4 on page 674 (Table A4.2). The International (or Hermann–Mauguin) symbol for a symmorphic space group consists of the centering symbol of the Bravais lattice (P, A, B, C, R, I, or F), followed by the point group symbol. It is not necessary to include the crystal system in the symbol, since this should be obvious from the point group (see Table 1.5).

The remaining $230 - 73 = 157$ space groups are obtained by systematically replacing every rotation axis in the point groups by all possible screw axes, and every mirror plane by all possible glide planes consistent with the Bravais lattice. These groups all have either a glide plane or a screw axis or both in their symbols, and they are known as the *non-symmorphic space groups*. They are ranked by point group in Appendix A4, Table A4.3 (page 675). Several space groups are defined with respect to two different origins, known as *first setting* and *second setting*; they are indicated in the tables by an asterisk after the space group symbol. In addition

some of the trigonal space groups can be defined with respect to either a hexagonal or a rhombohedral reference frame (see Section 1.7.3) and, hence, also have two settings.

For a rather extensive derivation of the space groups and a description of some of their uses in materials science we refer to Burns and Glazer [BG90]. The complete tables of all point and space groups can be found in the *International Tables for Crystallography*, Volume A [Hah96]. This book, and its companion volumes on reciprocal space [Shm96], and mathematical, physical, and chemical tables [WP99], are amongst the most important reference works for electron microscopists and crystallographers. When working on a crystallographic problem one should always keep them at hand.

It is now a straightforward matter to compute the coordinates of all points $\mathbf{r}^{(k)}$, $k = 2, \dots, N$ equivalent to a given point $\mathbf{r}^{(1)}$, i.e. the members of the *orbit*. All that is required is a list of N 4×4 transformation matrices corresponding to all the symmetry elements of the space group.[†] Multiplication of each matrix with the normal coordinates of the first point then results in a list of equivalent points. If the original point lies on one or more of the symmetry elements of the space group, then there will be duplicate entries in this list, and they will need to be removed. The largest possible multiplicity $N = 192$ is encountered in the face-centered cubic space group **Fm $\bar{3}$ m**. Although all symmetry operators for all space groups are explicitly listed in the *International Tables for Crystallography*, Vol. A, it is not advisable to enter all these matrices into a computer program. Through the clever use of group theory one can store all the necessary space group information in a surprisingly small number of bytes, as is discussed in detail in Section 1.9.3.

1.7 Coordinate transformations

The mathematical relations derived in this chapter allow us to compute any geometrical quantity in any of the seven crystal systems. One may now ask the question: how do these relations change when we change the reference frame? The need to change from one reference frame to another arises frequently in the study of solid state phase transformations, when the crystal structure changes with temperature or applied field (electric or magnetic). In addition, in the presence of planar defects, such as twins, it is frequently necessary to express crystallographic quantities on one side of the defect in the reference frame of the crystal on the other side. In this section we will describe in detail how one can convert vectors and the metric tensors from one reference frame to another one.

[†] That is, all the elements within the fundamental unit cell; neighboring unit cells can be reached by adding Bravais translation vectors to all equivalent points.

1.7.1 Transformation rules

Let us consider two crystallographic reference frames, $\{\mathbf{a}_1, \mathbf{a}_2, \mathbf{a}_3\}$ and $\{\mathbf{a}'_1, \mathbf{a}'_2, \mathbf{a}'_3\}$. In general, the relation between the two sets of basis vectors can be written as

$$\left. \begin{aligned} \mathbf{a}'_1 &= \alpha_{11}\mathbf{a}_1 + \alpha_{12}\mathbf{a}_2 + \alpha_{13}\mathbf{a}_3; \\ \mathbf{a}'_2 &= \alpha_{21}\mathbf{a}_1 + \alpha_{22}\mathbf{a}_2 + \alpha_{23}\mathbf{a}_3; \\ \mathbf{a}'_3 &= \alpha_{31}\mathbf{a}_1 + \alpha_{32}\mathbf{a}_2 + \alpha_{33}\mathbf{a}_3. \end{aligned} \right\} \quad (1.43)$$

This is a *linear* relation, known as a *coordinate transformation*. We will assume throughout this book that the origin itself does not change during the coordinate transformation. If there were a change in the position of the origin as well, then we would need to add a translation vector to the equations above.

The nine numbers α_{ij} can be grouped as a square matrix:

$$\alpha_{ij} = \begin{pmatrix} \alpha_{11} & \alpha_{12} & \alpha_{13} \\ \alpha_{21} & \alpha_{22} & \alpha_{23} \\ \alpha_{31} & \alpha_{32} & \alpha_{33} \end{pmatrix}, \quad (1.44)$$

and the transformation equations can be rewritten in short form as

$$\mathbf{a}'_i = \alpha_{ij}\mathbf{a}_j. \quad (1.45)$$

The *inverse* transformation must also exist and is described by the inverse of the matrix α_{ij} :

$$\mathbf{a}_i = \alpha_{ij}^{-1}\mathbf{a}'_j. \quad (1.46)$$

Consider the position vector \mathbf{p} . This vector is independent of the reference frame, and has components in both the unprimed and primed reference frames. We must have the following relation:

$$\mathbf{p} = p_i\mathbf{a}_i = p'_j\mathbf{a}'_j. \quad (1.47)$$

Using the inverse coordinate transformation we can rewrite the first equality as

$$p_i\mathbf{a}_i = p_i\alpha_{ij}^{-1}\mathbf{a}'_j,$$

and after comparison with the last equality of equation (1.47) we find

$$p'_j = p_i\alpha_{ij}^{-1}. \quad (1.48)$$

Note the order of the indices of the matrix α ; the summation index is the index i , which means that we must *premultiply* the matrix by the *row vector* p_i . Similarly, one can readily show that

$$p_i = p'_j\alpha_{ji}. \quad (1.49)$$

We interpret equations (1.48) and (1.49) as follows: the vector \mathbf{p} is independent of the chosen reference frame if its components with respect to two different reference frames are related to each other by equations (1.48) and (1.49). This relation obviously also holds for direction vectors $[uvw]$, since they are a special case of position vectors \mathbf{p} (integer components instead of rational ones).

It is now straightforward to derive the transformation relation for the direct metric tensor:

$$\begin{aligned} g'_{ij} &= \mathbf{a}'_i \cdot \mathbf{a}'_j; \\ &= \alpha_{ik} \mathbf{a}_k \cdot \alpha_{jl} \mathbf{a}_l; \\ &= \alpha_{ik} \alpha_{jl} \mathbf{a}_k \cdot \mathbf{a}_l, \end{aligned}$$

and hence

$$g'_{ij} = \alpha_{ik} \alpha_{jl} g_{kl}. \quad (1.50)$$

The inverse relation is given by

$$g_{ij} = \alpha_{ik}^{-1} \alpha_{jl}^{-1} g'_{kl}. \quad (1.51)$$

One can use these relations to *define* a second-rank tensor: any mathematical quantity h_{ij} which satisfies the above transformation rules is a second-rank tensor. Similarly, any mathematical quantity p_i , satisfying the transformation rules (1.48) and (1.49), is a vector. It is straightforward to extend these definitions to higher-order tensors, but we will not need them in this book. For a detailed overview of tensor calculus we refer to [Wre72].

Next, we will derive the transformation relations for quantities in reciprocal space. We have already seen that if the components of a vector \mathbf{p} are known in direct space, then its components in the reciprocal reference frame are given by

$$p_i^* = g_{ij} p_j.$$

Using equation (1.49) we have

$$p_i^* = g_{ij} \alpha_{kj} p'_k. \quad (1.52)$$

From equation (1.51) we find, after multiplying both sides of the equation by α_{kj} ,

$$g_{ij} \alpha_{kj} = \alpha_{il}^{-1} g'_{lk},$$

and substitution in equation (1.52) leads to

$$\begin{aligned} p_i^* &= \alpha_{il}^{-1} g'_{lk} p'_k, \\ &= \alpha_{il}^{-1} p_l'^*, \end{aligned}$$

where we have once again used the properties of the direct metric tensor. The components of a vector in reciprocal space thus transform as follows:

$$p_i^* = \alpha_{il}^{-1} p_l'^*, \quad (1.53)$$

and the inverse relation is given by

$$p_l'^* = \alpha_{li} p_i^*. \quad (1.54)$$

In particular, these equations are valid for the reciprocal lattice vectors \mathbf{g} .

The reciprocal basis vectors satisfy similar transformation relations, which are derived as follows:

$$\begin{aligned} \mathbf{g} &= g_i^* \mathbf{a}_i^* = g_l'^* \mathbf{a}_l'^*, \\ &= \alpha_{li} g_i^* \mathbf{a}_l'^*, \end{aligned}$$

from which we find:

$$\mathbf{a}_i^* = \mathbf{a}_l'^* \alpha_{li}. \quad (1.55)$$

The corresponding inverse relation is given by

$$\mathbf{a}_i'^* = \mathbf{a}_j^* \alpha_{ji}^{-1}. \quad (1.56)$$

Finally, it is again easy to show that the reciprocal metric tensor transforms according to the rules

$$g_{ij}^* = \alpha_{ki} \alpha_{lj} g_{kl}', \quad (1.57)$$

and

$$g_{ij}' = \alpha_{ki}^{-1} \alpha_{lj}^{-1} g_{kl}^*. \quad (1.58)$$

The transformation rules derived in this section are summarized in Table 1.6. All that is required to carry out *any* coordinate transformation is the matrix α_{ij} , expressing the new basis vectors in terms of the old ones. The relations in Table 1.6 require, in addition to α_{ij} , the inverse α_{ij}^{-1} and transpose α_{ij}^T matrices, and the transpose of the inverse matrix $(\alpha_{ij}^{-1})^T$. These transformation rules seem easy enough, but one must actually pay close attention to the indices in order to avoid mistakes. In the following subsection we will illustrate coordinate transformations by means of a few examples.

1.7.2 Examples of coordinate transformations

Example 1.15 Consider the two sets of basis vectors shown in Fig. 1.20; write down the transformation matrix α_{ij} . Show by explicit computation using the relations in

Table 1.6. Overview of all transformation relations for vectors and the metric tensor in direct and reciprocal space. Pay close attention to the order of the indices!

Quantity	Old to new	New to old
Direct basis vectors	$\mathbf{a}'_i = \alpha_{ij} \mathbf{a}_j$	$\mathbf{a}_i = \alpha_{ij}^{-1} \mathbf{a}'_j$
Direct metric tensor	$g'_{ij} = \alpha_{ik} \alpha_{jl} g_{kl}$	$g_{ij} = \alpha_{ik}^{-1} \alpha_{jl}^{-1} g'_{kl}$
Direct space vectors	$p'_i = p_j \alpha_{ji}^{-1}$	$p_i = p'_j \alpha_{ji}$
Reciprocal basis vectors	$\mathbf{a}^*_i = \mathbf{a}^*_j \alpha_{ji}^{-1}$	$\mathbf{a}^*_i = \mathbf{a}^*_j \alpha_{ji}$
Reciprocal metric tensor	$g'^*_{ij} = g^*_{kl} \alpha_{ki}^{-1} \alpha_{lj}$	$g^*_{ij} = g'^*_{kl} \alpha_{ki} \alpha_{lj}$
Reciprocal space vectors	$k'^*_i = \alpha_{ij} k^*_j$	$k^*_i = \alpha_{ij}^{-1} k'^*_j$

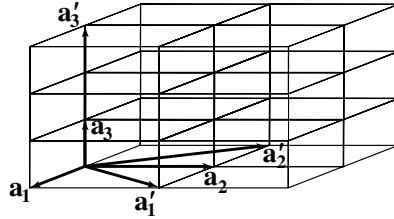


Fig. 1.20. Unit cell drawing for Example 1.15.

Table 1.6 how the $[uvw]$ direction and the (hkl) plane normal change to their new values in the primed reference frame.

Answer: The transformation matrix α_{ij} is easily derived from a visual inspection of Fig. 1.20:

$$\alpha_{ij} = \begin{pmatrix} 1 & 1 & 0 \\ -1 & 1 & 0 \\ 0 & 0 & 3 \end{pmatrix}.$$

Direction indices transform according to the inverse of this matrix, or

$$\begin{aligned} [u'v'w'] &= [uvw] \alpha_{ji}^{-1}; \\ &= \frac{1}{2} [uvw] \begin{pmatrix} 1 & -1 & 0 \\ 1 & 1 & 0 \\ 0 & 0 & \frac{2}{3} \end{pmatrix}; \\ &= \left[\frac{u+v}{2} \frac{v-u}{2} \frac{w}{3} \right]. \end{aligned}$$